Resource Allocation for Intelligent Reflecting Surface Aided Wireless Powered Mobile Edge Computing in OFDM Systems

Tong Bai, *Member, IEEE*, Cunhua Pan, *Member, IEEE*, Hong Ren, *Member, IEEE*, Yansha Deng, *Member, IEEE*, Maged Elkashlan, *Member, IEEE*, and Arumugam Nallanathan, *Fellow, IEEE*

Abstract—Wireless powered mobile edge computing (WP-MEC) has been recognized as a promising technique to provide both enhanced computational capability and sustainable energy supply to massive low-power wireless devices. However, its energy consumption becomes substantial, when the transmission link used for wireless energy transfer (WET) and for computation offloading is hostile. To mitigate this hindrance, we propose to employ the emerging technique of intelligent reflecting surface (IRS) in WP-MEC systems, which is capable of providing an additional link both for WET and for computation offloading. Specifically, we consider a multi-user scenario where both the WET and the computation offloading are based on orthogonal frequency-division multiplexing (OFDM) systems. Built on this model, an innovative framework is developed to minimize the energy consumption of the IRS-aided WP-MEC network, by optimizing the power allocation of the WET signals, the local computing frequencies of wireless devices, both the sub-band-device association and the power allocation used for computation offloading, as well as the IRS reflection coefficients. The major challenges of this optimization lie in the strong coupling between the settings of WET and of computing as well as the unit-modules constraint on IRS reflection coefficients. To tackle these issues, the technique of alternating optimization is invoked for decoupling the WET and computing designs, while two sets of locally optimal IRS reflection coefficients are provided for WET and for computation offloading separately relying on the successive convex approximation method. The numerical results demonstrate that our proposed scheme is capable of monumentally outperforming the conventional WP-MEC network without IRSs. Quantitatively, about 80% energy consumption reduction is attained over the conventional MEC system in a single cell, where 3 wireless devices are served via 16 sub-bands, with the aid of an IRS comprising of 50 elements.

Index Terms—Intelligent reflecting surface (IRS), wireless powered mobile edge computing (WP-MEC), orthogonal frequency-division multiplexing (OFDM).

I. INTRODUCTION

A. Motivation and Scope

IN THE Internet-of-Things (IoT) era, a myriad of heterogeneous devices are envisioned to be interconnected [1]. However, due to the stringent constraints both on device sizes and on manufacturing cost, many of them have to be equipped with either life-limited batteries or low-performance processors. Consequently, if only relying on their local computing, these resource-constrained devices are incapable of accommodating the applications that require sustainable and low-latency computation, e.g. wireless body area networks [2] and environment monitoring [3]. Fortunately, wireless powered mobile edge computing (WP-MEC) [4]–[13], which incorporates radio frequency (RF) based wireless energy transmission (WET) [14]–[16] and mobile edge computing (MEC) [17], [18], constitutes a promising solution of this issue. Specifically, at the time of writing, the commercial RF-based WET has already been capable of delivering 0.05 mW to a distance of $12-14$ m [14], which is sufficient to charge many low-power devices, whilst the MEC technique may provide the cloud-like computing service at the edge of mobile networks [18]. In WP-MEC systems, hybrid access points (HAP) associated with edge computing nodes are deployed in the proximity of wireless devices, and the computation of these devices is typically realized in two phases, namely the WET phase and the computing phase. To elaborate, the batteries of the devices are replenished by harvesting WET signals from the HAP in the first phase, while in the computing phase, devices may decide whether to process their computational tasks locally or offload them to edge computing nodes via the HAP.

Given that these wireless devices are fully powered by WET in WP-MEC systems, the power consumption at HAPs becomes substantial, which inevitably increases the expenditure on energy consumption and may potentially saturate power rectifiers. At the time of writing, the existing research

contributions that focus on reducing the power consumption mainly rely on the joint optimization of the WET and of computing [5], as well as cooperative computation offloading [10], [11]. However, wireless devices are still suspicious to severe channel attenuation, which limits the performance of WP-MEC systems. To resolve this issue, we propose to deploy the emerging intelligent reflecting surfaces (IRS) [19]–[21] in the vicinity of devices, for providing an additional transmission link both for WET and for computation offloading. Then, the power consumption can be beneficially reduced both for the downlink and for the uplink. To elaborate, an IRS comprises of an IRS controller and a large number of low-cost passive reflection elements. Regulated by the IRS controller, each IRS reflection element may adapt both the amplitude and the phase of the incident signals reflected, for collaboratively modifying the signal propagation environment. The gain attained by IRSs is based on the combination of so-called the virtual array gain and the reflection-enabled beamforming gain [19]. More explicitly, the virtual array gain is achieved by combining the direct and IRS-reflected links, while the reflection-enabled beamforming gain is realized by proactively adjusting the reflection coefficients of the IRS elements. By combining these two types of gain together, IRSs are capable of reducing the power required both for WET and for computation offloading, thus improving the energy efficiency of WP-MEC systems. In this treatise, we aim for providing a holistic scheme to minimize the energy consumption of WP-MEC systems, relying on IRSs.

B. Related Works

The current state-of-the-art contributions are reviewed from the perspectives of WP-MEC and of IRS-aided networks, as follows.

1) Wireless Powered Mobile Edge Computing: This topic has attracted an increasing amount of research attention [4]–[13]. Specifically, You *et al.* firstly proposed the WP-MEC framework [4], where the probability of successfully computing was maximized subject to the constraints both on energy harvesting and on latency. The single-user system considered in this first trial limits its application in large-scale scenarios. For eliminating this shortage, an energy-minimization algorithm was proposed for the multi-user scenario [5], where the devices' computation offloading was realized by the time division multiple access (TDMA) technique. Following this, Bi and Zhang maximized the weighted sum computation rate in a similar TDMA system [6], while an orthogonal frequency division multiple access (OFDMA) based multi-user WP-MEC system was investigated in [7]. A holistic online optimization algorithm was proposed for the WP-MEC in industrial IoT scenarios [8]. In the aforementioned works, the associated optimization is commonly realized with the aid of the alternating optimization (AO) method, because the pertinent optimization problems are usually not jointly convex. This inevitably imposes a delay on decision making. To mimic this issue, Huang *et al.* proposed a deep reinforcement learning based algorithm for maximizing the computation rate of WP-MEC systems [9], which may replace the aforementioned complicated optimization by a pre-trained look-up table. Furthermore, as for the system where both near and far devices have to be served, the energy consumption at the HAP has to be vastly increased, because the farther device harvests less energy while a higher transmit power is required for its computation offloading. Aimed for releasing this so-called "doubly near-far" issue, the technique of user cooperation was revisited [10], [11]. At the time of writing, the WET and computation offloading in WP-MEC systems in the face of hostile communication environments has not been well addressed. Against this background, we aim for tackling this issue by invoking IRSs. Let us now continue by reviewing the relevant research contributions on IRSs as follows.

2) IRS-Aided Networks: In order to exploit the potential of IRSs, an upsurging number of research efforts have been devoted in its channel modeling [22], [23], analyzing the impact of limited-resolution phase shifts [24], [25], channel estimation [26], [27] as well as IRS reflection coefficient designs [28]–[31]. Inspired by these impressive research contributions, the advantageous effect of IRSs was evaluated in various application scenarios [32]–[41]. Specifically, an IRS was employed in multi-cell communications systems for mitigate the severe inter-cell interference [32], where an IRS comprising of 100 reflection elements was shown to be capable of doubling the sum rate of the multi-cell system. Yang *et al.* investigated an IRS-enhanced OFDMA system [33], whose common rate was improved from around 2.75 bps/Hz to 4.4 bps/Hz, with the aid of a 50-element IRS. Apart from assisting the aforementioned throughput maximization in the conventional communications scenario, a sophisticated design of IRSs may also eminently upgrade the performance of diverse emerging wireless networks, e.g. protecting data transmission security [34], [35], enhancing the user cooperation in wireless powered communications networks [36], reducing the latency in IRS-aided MEC systems [37], as well as assisting energy harvesting systems [38]–[41].[1] These impressive research contributions inspire us to exploit the beneficial role of IRSs in this momentous WP-MEC scenario.

C. Novelty and Contributions

In this paper, an innovative IRS-aided WP-MEC framework is proposed, where we consider orthogonal frequency-division multiplexing (OFDM) systems for its WET and devices' computation offloading. Under this framework, a joint WET and computing design is conceived for minimizing its energy consumption, by optimizing the power allocation of the WET signals over OFDM sub-bands, the local computing frequencies of wireless devices, both the sub-band-device association and the power allocation used for computation offloading, as well as the pertinent IRS reflection coefficient design. Let us now detail our contributions as follows.

---

[1]As for IRS-aided energy harvesting systems, the beneficial role of IRSs has been investigated in simultaneous wireless information and power transfer (SWIPT) systems [38]–[40] and wireless powered communications networks [41]. However, the advantageous effect of IRSs has not been exploited in WP-MEC systems. In this paper, we aim at filling this gap. Since the IRS reflection coefficient design is coupled with the optimization of resource allocation and of computation offloading, they have to be jointly optimized, which deserves a specific study.

- *Energy minimization problem formulation for the new IRS-aided WP-MEC design:* In order to reduce the energy consumption of WP-MEC systems, we employ an IRS in WP-MEC systems and formulate a pertinent energy minimization problem. Owing to the coupling effects between the designs of WET and of computing, it is difficult to find its globally optimal solution. Alternatively, we provide an alternating optimization (AO) based solution to approach a locally optimal solution, by iteratively optimizing settings of WET and of computing.

- *WET design:* The WET setting is realized by alternatively optimizing the power allocation of energy-carrying signals over OFDM sub-bands and the IRS reflection coefficients. Specifically, given a set of fixed IRS reflection coefficients, the power allocation problem can be simplified to be a linear programming problem, which can be efficiently solved by the existing optimization software. Given a fixed power allocation, the IRS reflection coefficient design becomes a feasibility-check problem, the solution of which is incapable of ensuring a rapid convergence. To tackle this issue, we reformulate the problem by introducing a number of auxiliary variables, and provide a locally optimal design of IRS reflection coefficients, with the aid of several steps of mathematical manipulations and of the successive convex approximation (SCA) method.

- *Computing design:* The settings at the computing phase are specified by alternatively optimizing the joint sub-band-device association for and the power allocation for devices' computation offloading, IRS reflection coefficients at the computing phase as well as the local computing frequencies. Specifically, as verified by [42], the duality gap vanishes when the number of sub-bands exceeds 8. Hence, we provide a near-optimal solution for the joint sub-band-device association and power allocation problem, relying on the Lagrangian duality method. The IRS reflection coefficients are designed using the similar approach devised for that in the WET phase. Finally, our analysis reveals that the optimal local computing frequencies can be obtained by selecting their maximum allowable values.

- *Numerical validations:* Our numerical results validates the benefits of employing IRSs in WP-MEC systems, and quantify the energy consumption of our proposed framework in diverse simulation environments, together with two benchmark schemes.

The rest of the paper is organized as follows. In Section II, we describe the system model and formulate the pertinent problem. A solution of this problem is provided in Section III. The numerical results are presented in Section IV. Finally, our conclusions are drawn in Section V.

Notation: In this paper, scalars are denoted by italic letters. Boldface lower- and upper-case letters denote vectors and matrices, respectively; $\mathbb{C}^{M \times N}$ represents the space of $M \times N$ complex matrices; $\boldsymbol{I}_N$ denotes an $N \times N$ identity matrix; j denotes the imaginary unit, i.e. $j^2 = -1$. The maths operations used throughout the paper are summarized in Table I.

TABLE I
MATH OPERATIONS

| Notation	Operation
$\boldsymbol{x}^H$	the Hermitian transpose of $\boldsymbol{x}$
$\boldsymbol{X}^H$	the Hermitian transpose of $\boldsymbol{X}$
$\boldsymbol{X}^{-1}$	the inverse of $\boldsymbol{X}$
$\lvert \cdot \rvert$	the absolute value of a scalar
$\lVert \cdot \rVert$	the 2-norm of a vector
$\mathrm{diag}(\boldsymbol{x})$	the diagonal matrix where the diagonal elements are $\boldsymbol{x}$
$\mathrm{diag}(\boldsymbol{X})$	the vector whose elements are the diagonal elements of $\boldsymbol{X}$
$\mathcal{CN}(0, \sigma^2)$	Circularly Symmetric Complex Gaussian associated with zero-mean and variance σ^2
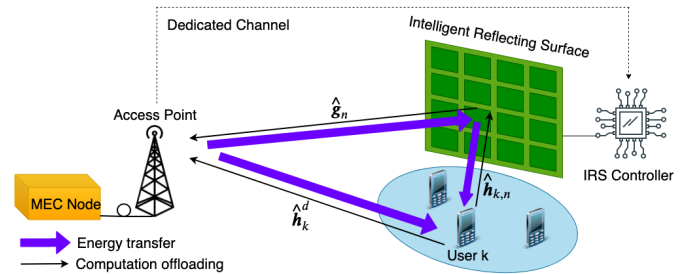
Fig. 1. An illustration of our IRS-aided WP-MEC system, where K single-antenna devices are served by a mobile edge computing node via a single-antenna hybrid access point, with the aid of an N-element IRS.
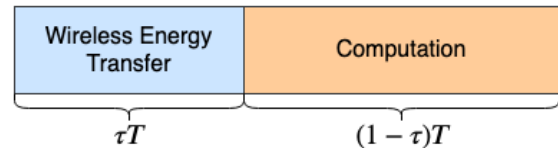
Fig. 2. An illustration of the harvest-then-computing protocol, where τT and $(1 - \tau)T$ refer to the duration of the WET and the computing phases, respectively.

II. SYSTEM MODEL AND PROBLEM FORMULATION

As illustrated in Fig. 1, we consider an OFDM-based WP-MEC system, where K single-antenna devices are served by a single-antenna hybrid access point (HAP) associated with an edge computing node through M equally-divided OFDM sub-bands. Similar to the assumption in [5]–[7], we assume that these devices do not have any embedded energy supply available, but are equipped with energy storage devices, e.g. rechargeable batteries or super-capacitors, for storing the energy harvested from RF signals. As shown in Fig. 2, relying on the so-called "harvest-then-computing" mechanism [5], the system operates in a two-phase manner in each time block. Specifically, during the WET phase, the HAP broadcasts energy-carrying signals to all K devices for replenishing their batteries, while these K devices process their computing tasks both by local computing and by computation offloading during the computing phase. We denote the duration of each time block by T, which is chosen to be no larger than the tolerant latency of MEC applications. The duration of the WET and of the computing phases are set as τT and $(1 - \tau)T$,

respectively. Furthermore, to assist the WET and the devices' computation offloading in this WP-MEC system, we place an IRS comprising of N reflection elements in the proximity of devices. The reflection coefficients of these IRS reflection elements are controlled by an IRS controller in a real-time manner, based on the optimization results provided by the HAP.

Let us continue by elaborating on the equivalent baseband time-domain channel as follows. We denote the equivalent baseband time-domain channel of the direct link between the k-th device and the HAP, the equivalent baseband time-domain channel between the n-th IRS element and the HAP, and the equivalent baseband time-domain channel between the k-th device and the n-th IRS element by $\hat{\boldsymbol{h}}_k^d \in \mathbb{C}^{L_k^d \times 1}$, $\hat{\boldsymbol{g}}_n \in \mathbb{C}^{L_1 \times 1}$ and $\hat{\boldsymbol{r}}_{k,n} \in \mathbb{C}^{L_{2,k} \times 1}$, respectively, where L_k^d, L_1 and $L_{2,k}$ represent the respective number of delay spread taps. Without loss of generality, we assume that the above channels remain approximately constant over each time block. Furthermore, the channels are assumed to be reciprocal for the downlink and the uplink.

As for the IRS, we denote the phase shift vector of and the amplitude response of the IRS reflection elements by $\boldsymbol{\theta} = [\theta_1, \theta_2, \dots, \theta_N]^T$ and $\boldsymbol{\beta} = [\beta_1, \beta_2, \dots, \beta_N]^T$, respectively, where we have $\theta_n \in [0, 2\pi)$ and $\beta_n \in [0, 1]$. Then, the corresponding reflection coefficients of the IRS are given by $\boldsymbol{\Theta} = [\Theta_1, \Theta_2, \dots, \Theta_N]^T = [\beta_1\,e^{j\theta_1}, \beta_2\,e^{j\theta_2}, \dots, \beta_N e^{j\theta_N}]^T$, where j represents the imaginary unit and we have $|\Theta_n| \leq 1$ for $\forall n \in \mathcal{N}$. The baseband equivalent time-domain channel of the reflection link is the convolution of the device-IRS channel, of the IRS reflection response, and of the IRS-HAP channel. Specifically, the baseband equivalent time-domain channel reflected by the n-th IRS element is formulated as $\hat{\boldsymbol{h}}_{k,n}^r = \hat{\boldsymbol{r}}_{k,n} * \Theta_n * \hat{\boldsymbol{g}}_n = \Theta_n \hat{\boldsymbol{r}}_{k,n} * \hat{\boldsymbol{g}}_n$. Here, we have $\hat{\boldsymbol{h}}_{k,n}^r \in \mathbb{C}^{L_k^r \times 1}$ and $L_k^r = L_1 + L_{2,k} - 1$, which denotes the number of delay spread taps of the reflection channel. Furthermore, we denote the time-domain zero-padded concatenated device-IRS-HAP channel between the k-th device and the HAP via the n-th IRS element by $\boldsymbol{v}_{k,n} = [(\hat{\boldsymbol{r}}_{k,n} * \hat{\boldsymbol{g}}_n)^T, 0, \dots, 0]^T \in \mathbb{C}^{M \times 1}$. Upon denoting $\boldsymbol{V}_k = [\boldsymbol{v}_{k,1}, \dots, \boldsymbol{v}_{k,N}] \in \mathbb{C}^{M \times N}$, we formulate the composite device-IRS-HAP channel between the k-th device and the HAP as $\boldsymbol{h}_k^r = \boldsymbol{V}_k \boldsymbol{\Theta}$. Similarly, we use $\boldsymbol{h}_k^d = [(\hat{\boldsymbol{h}}_k^d)^T, 0, \dots, 0]^T \in \mathbb{C}^{M \times 1}$ to represent the zero-padded time-domain channel of the direct device-HAP link. To this end, we may readily arrive at the superposed channel impulse response (CIR) for the k-th device, formulated as

$$\boldsymbol{h}_k = \boldsymbol{h}_k^d + \boldsymbol{h}_k^r = \boldsymbol{h}_k^d + \boldsymbol{V}_k \boldsymbol{\Theta}, \quad \forall k \in \mathcal{K}, \tag{1}$$

whose number of delay spread taps is given by $L_k = \max(L_k^d, L_k^r)$. We assume that the number of cyclic prefixes (CP) is no smaller than the maximum number of delay spread taps for all devices, so that the inter-symbol interference (ISI) can be eliminated. Upon denoting the m-th row of the $M \times M$ discrete Fourier transform (DFT) matrix $\boldsymbol{F}_M$ by $\boldsymbol{f}_m^H$, we formulate the channel frequency response (CFR) for the k-th device at the m-th sub-band as

$$C_{k,m}(\boldsymbol{\Theta}) = \boldsymbol{f}_m^H \boldsymbol{h}_k = \boldsymbol{f}_m^H \boldsymbol{h}_k^d + \boldsymbol{f}_m^H \boldsymbol{V}_k \boldsymbol{\Theta}, \quad \forall k \in \mathcal{K}, \forall m \in \mathcal{M}. \tag{2}$$

For ease of exposition, we assume that the knowledge of $\boldsymbol{h}_k^d$ and of $\boldsymbol{V}_k$ is perfectly known at the HAP. Naturally, this assumption is idealistic. Hence, the algorithm developed in this paper can be deemed to represent the best-case bound for the energy performance of realistic scenarios. Since different types of signals are transmitted in the WET and computing phases, the reflection coefficients of the IRS require separate designs in these two phases. The models of the WET and of computing phases are detailed as follows.

A. Model of the Wireless Energy Transfer Phase

It is assumed that the capacity of devices' battery is large enough so that all the harvest energy can be saved without energy overflow. Let us use $\boldsymbol{\Theta}^E = \{\Theta_1^E, \Theta_2^E, \dots, \Theta_N^E\}$ to represent the IRS reflection-coefficient vector during the WET phase, where we have $|\Theta_n^E| \leq 1$ for $\forall n \in \mathcal{N}$. Then, the composite channel of the m-th sub-band for the k-th device during the WET phase $C_{k,m}(\boldsymbol{\Theta}^E)$ can be obtained by (2). As a benefit of the broadcasting nature of WET, each device can harvest the energy from the RF signals transmitted over all M sub-bands. Hence, upon denoting the power allocation for the energy-carrying RF signals at the M sub-bands during the WET phase by $\boldsymbol{p}^E = [p_1^E, p_2^E, \dots, p_M^E]$, we are readily to formulate the energy harvested by the k-th device as [5]

$$E_k(\tau, \boldsymbol{p}^E, \boldsymbol{\Theta}^E) = \sum_{m=1}^{M} \eta \tau T p_m^E |C_{k,m}(\boldsymbol{\Theta}^E)|^2, \tag{3}$$

where $\eta \in [0, 1]$ denotes the efficiency of the energy harvesting at the wireless devices.[2] Due to the broadcasting nature of wireless energy transfer, the energy harvested at specific wireless devices might be higher than that required. It is assumed that the redundant energy is dropped at the end of each time slot.

B. Model of the Computing Phase

We consider the data-partitioning based application [46], where a fraction of the data can be processed locally, while the other part can be offloaded to the edge node. For a specific time block, we use L_k and ℓ_k to denote the number of bits to be processed by the k-th device and its computation offloading volume in terms of the number of bits, respectively. The models of local computing, of computation offloading and of edge computing are detailed as follows.

1) Local Computing: We use f_k and c_k to represent its computing capability in terms of the number of central processing unit (CPU) cycles per second and the number of CPU cycles required to process a single bit, for the k-th device, respectively. The number of bits processed by local computing is readily calculated as $(1 - \tau)T f_k / c_k$, and the number of

---

[2]The energy conversion is generally a non-linear process [43]–[45], and the energy conversion efficiency highly depends on both the input power and signal waveform. It was shown that when the input power is smaller than a certain saturation level, the energy conversion process can be nicely approximated as a linear function [43]–[45], which may achieve a reasonable trade-off between the physically tangible presentation and the mathematical tractability. As an initial investigation, we assume the energy harvesting model as a linear process. The extension concerning the non-linear energy harvesting model will be considered in our future work.

bits to be offloaded is given by $\ell_k = L_k - (1-\tau)Tf_k/c_k$. Furthermore, we assume that f_k is controlled in the range of $[0, f_{max}]$ using the dynamic voltage scaling model [46]. Upon denoting the computation energy efficiency coefficient of the processor's chip by κ, we formulate the power consumption of the local computing mode as κf_k^2 for the k-th device [46].

2) Computation Offloading: In order to mitigate the co-channel interference, the devices' computation offloading is realized relying on the orthogonal frequency-division multiple access (OFDMA) scheme. In this case, each sub-band is allowed to be used by at most a single device. We use the binary vector $\boldsymbol{\alpha}_k = [\alpha_{k,1}, \alpha_{k,2}, \ldots, \alpha_{k,M}]^T$ and the non-negative vector $\boldsymbol{p}_k^I = [p_{k,1}^I, p_{k,2}^I, \ldots, p_{k,M}^I]^T$ to represent the association between the sub-band and devices as well as the power allocation of the k-th device to the M sub-bands, respectively, where we have

$$\alpha_{k,m} = \begin{cases} 0, & \text{if } p_{k,m}^I = 0, \\ 1, & \text{if } p_{k,m}^I > 0. \end{cases} \quad (4)$$

The power consumption of computation offloading is given by $\sum_{m=1}^M \alpha_{k,m}(p_{k,m} + p_c)$, where p_c represents a constant circuit power (caused by the digital-to-analog converter, filter, etc.) [5]. Let us denote the IRS reflection-coefficient vector during the computation offloading by $\boldsymbol{\Theta}^I = \{\Theta_1^I, \Theta_2^I, \ldots, \Theta_N^I\}$, where $|\Theta_n^I| \leq 1$ for $\forall n \in \mathcal{N}$. Then, the composite channel of the k-th device at the m-th sub-band denoted by $C_{k,m}(\boldsymbol{\Theta}^I)$ can be obtained by (2). The corresponding achievable rate of computation offloading is formulated below for the k-th device

$$R_k(\boldsymbol{\alpha}_k, \boldsymbol{p}_k^I, \boldsymbol{\Theta}^I) = \sum_{m=1}^M \alpha_{k,m} B \log_2\left(1 + \frac{p_{k,m}|C_{k,m}(\boldsymbol{\Theta}^I)|^2}{\Gamma \sigma^2}\right), \quad (5)$$

where Γ is the gap between the channel capacity and a specific modulation and coding scheme, while σ^2 represents the variance of the additive white Gaussian noise during computation offloading. Furthermore, in order to offload all the ℓ_k bits within the duration of the computation phase, the achievable offloading rate has to obey $R_k(\tau, \boldsymbol{\alpha}_k, \boldsymbol{p}_k^I, \boldsymbol{\Theta}^I) \geq \frac{\ell_k}{(1-\tau)T}$.

3) Edge Computing: Invoking the simplified linear model [5], we formulate the energy consumption at the edge node as $\vartheta \sum_{k=1}^K \ell_k = \vartheta \sum_{k=1}^K [L_k - (1-\tau)Tf_k/c_k]$. Furthermore, the latency imposed by edge computing comprises of two parts. The first part is caused by processing the computational tasks. Given that edge nodes typically possess high computational capabilities, this part can be negligible. The second part is induced by sending back the computational results, which are usually of a small volume. Hence, the duration of sending the feedback is also negligible. As such, we neglect the latency induced by edge computing.

C. Problem Formulation

In this paper, we aim for minimizing the total energy consumption of the OFDM-based WP-MEC system, by optimizing the time allocation for WET and computing phases τ, both the power allocation $\boldsymbol{p}^E$ and the IRS reflection coefficients $\boldsymbol{\Theta}^E$ at the WET phase, and the local CPU frequency at devices $\boldsymbol{f}$,

the sub-band-device association $\{\boldsymbol{\alpha}_k\}$ and the power allocation $\{\boldsymbol{p}_k\}$ as well as the IRS reflection coefficients $\boldsymbol{\Theta}^I$ at the computing phase, subject to the energy constraint imposed by energy harvesting, the latency requirement of computation offloading and the sub-band-device association constraint in OFDMA systems as well as the constraint on IRS reflection coefficients. Since the batteries of all the wireless devices are replenished by the HAP, their energy consumption is covered by the energy consumption at the HAP during the WET phase. Hence, the total energy consumption of the system is formulated as the summation of the energy consumption both of the WET at the HAP and of the edge computing as well as of the circuit and controlling at the AP and IRS, i.e. $\tau T \sum_{m=1}^M p_m^E + \vartheta \sum_{k=1}^K [L_k - (1-\tau)Tf_k/c_k] + E_c$, where E_c represents the energy consumption of the circuit and controlling at the AP and IRS. Since the energy consumption of the circuit and controlling at the AP and IRS is typically a fixed value, the third term above can be neglected while the optimization is proceeded. To this end, the energy minimization problem is readily formulated for our OFDM-based WP-MEC system as

$$\mathcal{P}0: \min_{\substack{\tau, \boldsymbol{p}^E, \boldsymbol{\Theta}^E, \boldsymbol{f}, \\ \{\boldsymbol{\alpha}_k\}, \{\boldsymbol{p}_k^I\}, \boldsymbol{\Theta}^I}} \tau T \sum_{m=1}^M p_m^E + \vartheta \sum_{k=1}^K \left[L_k - \frac{(1-\tau)Tf_k}{c_k}\right]$$

$$\text{s.t.} \quad 0 < \tau < 1, \quad (6a)$$

$$p_m^E \geq 0, \quad \forall m \in \mathcal{M}, \quad (6b)$$

$$|\Theta_n^E| \leq 1, \quad \forall n \in \mathcal{N}, \quad (6c)$$

$$0 \leq f_k \leq f_{max}, \quad \forall k \in \mathcal{K}, \quad (6d)$$

$$\alpha_{k,m} \in \{0, 1\}, \quad \forall k \in \mathcal{K}, \quad \forall m \in \mathcal{M}, \quad (6e)$$

$$\sum_{k=1}^K \alpha_{k,m} \leq 1, \quad \forall m \in \mathcal{M}, \quad (6f)$$

$$p_{k,m}^I \geq 0, \quad \forall k \in \mathcal{K}, \quad \forall m \in \mathcal{M}, \quad (6g)$$

$$|\Theta_n^I| \leq 1, \quad \forall n \in \mathcal{N}, \quad (6h)$$

$$(1-\tau)T\left[\kappa f_k^2 + \sum_{m=1}^M \alpha_{k,m}(p_{k,m}^I + p_c)\right]$$
$$\leq E_k(\tau, \boldsymbol{p}^E, \boldsymbol{\Theta}^E), \quad \forall k \in \mathcal{K}, \quad (6i)$$

$$(1-\tau)TR_k(\boldsymbol{\alpha}_k, \boldsymbol{p}_k^I, \boldsymbol{\Theta}^I)$$
$$\geq L_k - \frac{(1-\tau)Tf_k}{c_k}, \quad \forall k \in \mathcal{K}. \quad (6j)$$

Constraint (6a) restricts the time allocation for the WET and for the computing phases. Constraint (6b) and (6c) represent the range of the power allocation and the IRS reflection coefficients at the WET phase, respectively. Constraint (6d) gives the range of tunable local computing frequencies. Constraint (6e) and (6f) detail the requirement of sub-band-device association in OFDMA systems. Constraint (6g) and (6h) restrict the range of the power allocation and the IRS reflection coefficient at the computing phase, respectively. Constraint (6i) indicates that the sum energy consumption of local computing and of computation offloading should not exceed the harvested energy for each device. Finally, Constraint (6j) implies that the communication link between the k-th device and the

HAP is capable of offloading the corresponding computational tasks within the duration of the computing phase.

III. JOINT OPTIMIZATION OF THE SETTINGS IN THE WET AND THE COMPUTING PHASES

In this section, we propose to solve Problem $\mathcal{P}0$ in a two-step procedure. Firstly, given a fixed $\hat{\tau} \in (0,1)$, Problem $\mathcal{P}0$ can be simplified as follows

$$\mathcal{P}1 : \min_{\substack{\boldsymbol{p}^E, \boldsymbol{\Theta}^E, \boldsymbol{f}, \\ \{\boldsymbol{\alpha}_k\}, \{\boldsymbol{p}_k^I\}, \boldsymbol{\Theta}^I}} \hat{\tau}T \sum_{m=1}^{M} p_m^E + \vartheta \sum_{k=1}^{K} \left[L_k - \frac{(1-\hat{\tau})Tf_k}{c_k} \right]$$

$$\text{s.t.} \quad (6b),(6c),(6d),(6e),(6f),(6g),(6h),(6i),(6j)$$

In the second step, we aim for finding the optimal $\hat{\tau}$ that is capable of minimizing the objective function (OF) of Problem $\mathcal{P}0$ using the one-dimensional search method.[3] In the rest of this section, we focus on solving Problem $\mathcal{P}1$. At a glance of Problem $\mathcal{P}1$, the optimization variables $\boldsymbol{f}$, $\{\boldsymbol{\alpha}_k\}$ and $\{\boldsymbol{p}_k^I\}$ are coupled with $\boldsymbol{p}^E$ and $\boldsymbol{\Theta}^E$ in Constraint (6i), which makes the problem difficult to solve. To tackle this issue, the AO technique is invoked. Specifically, upon initializing the setting of the computing phase, we may optimize the design of the WET phase while fixing the time allocation and the computing phase settings. Then, the computing phase settings could be optimized while fixing the time allocation and the design of the WET. A suboptimal solution can be obtained by iteratively optimizing the designs of the WET and of the computing phases. Let us detail the initialization as well as the designs of the WET and of the computing phases, as follows.

A. Initialization of the Time Allocation and the Computing Phase

In order to ensure our WET design to be a feasible solution of Problem $\mathcal{P}1$, the initial settings of the computing phase denoted by $\boldsymbol{f}^{(0)}, \{\boldsymbol{\alpha}_k^{(0)}\}, \{\boldsymbol{p}_k^{I(0)}\}, \boldsymbol{\Theta}^{I(0)}$ should satisfy Constraint (6d), (6e), (6f), (6g), (6h) and (6j). Without any loss of generality, their initialization is set as follows.

- Local computing frequency $\boldsymbol{f}^{(0)}$: Obeying the uniform distribution, each element of $\boldsymbol{f}^{(0)}$ is randomly set in the range of $[0, f_{max}]$.
- IRS reflection coefficient at the computing phase $\boldsymbol{\Theta}^{I(0)}$: Obeying the uniform distribution, the amplitude response $\beta_n^{I(0)}$ and the phase shift $\theta_n^{I(0)}$ are randomly set in the range of $[0, 1]$ and of $[0, 2\pi)$, respectively. Then, $\boldsymbol{\Theta}^{I(0)} = \{\beta_1^{I(0)} e^{j\theta_1^{I(0)}}, \ldots, \beta_N^{I(0)} e^{j\theta_N^{I(0)}}\}$ can be obtained.
- Sub-band-device association at the computing phase $\{\boldsymbol{\alpha}_k^{(0)}\}$: We reserve a single sub-band for the devices associated with the index ranging from $k = 1$ to $k = K$, sequentially. Specific to the k-th device, we use $k_m^{(0)}$ to denote the sub-band having the maximum $|C_{k,m}(\boldsymbol{\Theta}^{I(0)})|^2$ over the unassigned sub-bands, and assign this sub-band to the k-th device.

- Power allocation at the computing phase $\{\boldsymbol{p}_k^{I(0)}\}$: For the k-th device, its power allocation at the computing phase should satisfy Constraint (6j). For minimizing the energy consumption, we assume the equivalence of two sides in Constraint (6j). Then, its initial power allocation is given by $p_{k,k_m^{(0)}}^{I(0)} = \frac{\Gamma\sigma^2 \left[2^{\frac{L_k}{(1-\hat{\tau})TB} - \frac{f_k}{c_k B}} - 1 \right]}{\left| c_{k,k_m^{(0)}}(\boldsymbol{\Theta}^{I(0)}) \right|^2}$. For those sub-bands associated with the index $m \neq k_m^{(0)}$, we set $p_{k,m}^{I(0)} = 0$.

B. Design of the WET Phase While Fixing the Time Allocation and Computing Settings

Given a fixed time allocation $\hat{\tau}$ and the settings of the computing phase $\boldsymbol{f}$, $\{\boldsymbol{\alpha}_k\}$, $\{\boldsymbol{p}_k^I\}$ and $\boldsymbol{\Theta}^I$, we may simplify Problem $\mathcal{P}1$ as

$$\mathcal{P}2 : \min_{\boldsymbol{p}^E, \boldsymbol{\Theta}^E} \hat{\tau}T \sum_{m=1}^{M} p_m^E$$

$$\text{s.t.} \quad (6b),(6c),$$

$$(1-\hat{\tau})T \left[\kappa f_k^2 + \sum_{m=1}^{M} \alpha_{k,m}(p_{k,m}^I + p_c) \right]$$

$$\leq \sum_{m=1}^{M} \eta\hat{\tau}T p_m^E |C_{k,m}(\boldsymbol{\Theta}^E)|^2, \quad \forall k \in \mathcal{K}. \quad (8a)$$

Since Constraint (8a) is not jointly convex regarding $\boldsymbol{p}^E$ and $\boldsymbol{\Theta}^E$, we optimize one of these two variables while fixing the other in an iterative manner, relying on the AO technique, as follows.

1) Optimizing the Power Allocation of the WET Phase While Fixing the Settings of the Time Allocation, the Computing Phase and the IRS Reflection Coefficient at the WET Phase: Given an IRS phase shift design $\boldsymbol{\Theta}^E$, Problem $\mathcal{P}2$ is simplified as

$$\mathcal{P}2\text{-}1 : \min_{\boldsymbol{p}^E} \hat{\tau}T \sum_{m=1}^{M} p_m^E$$

$$\text{s.t.} \quad (6b),(8a). \quad (9a)$$

It can be observed that Problem $\mathcal{P}2$-1 is a linear programming problem, which can be readily solved with the aid of the general implementation of interior-point methods, e.g. CVX [47]. The complexity is given by $\sqrt{M + KM}M[M + KM^3 + M(M + KM^2) + M^2]$ [48], i.e. $\mathcal{O}(K^{1.5}M^{4.5})$.

2) Optimizing the IRS Reflection Coefficient at the WET Phase While Fixing the Settings of the Time Allocation, the Computing Phase and the Power Allocation at the WET Phase: Given a power allocation at the WET phase $\boldsymbol{p}^E$, Problem $\mathcal{P}2$ becomes a feasibility-check problem, i.e.

$$\mathcal{P}2\text{-}2 : \text{Find } \boldsymbol{\Theta}^E$$

$$\text{s.t.} \quad (6c),(8a). \quad (10a)$$

As verified in [28], if one of the sub-problems is a feasibility-check problem, the iterative algorithm relying on the AO technique has a slow convergence. Specific to the problem considered, the operation of Find in Problem $\mathcal{P}2$-2 cannot guarantee the OF of Problem $\mathcal{P}2$ to be further reduced in each

---

[3]One-dimensional search methods typically incurs high computational complexity. In practice, the time allocation can be proceeded offline based on the typical data set containing both channel information and volume of computational tasks, and then set as a fixed value.

iteration. To address this issue, we reformulate Problem $\mathcal{P}2$-2 as follows, by introducing a set of auxiliary variables $\{\xi_k\}$

$$\mathcal{P}2\text{-}2' : \max_{\Theta^E, \{\xi_k\}} \sum_{k=1}^{K} \xi_k$$
$$\text{s.t.} \quad (6c),$$

$$\xi_k + \kappa f_k^2 + \sum_{m=1}^{M} \alpha_{k,m}(p_{k,m}^I + p_c)$$
$$\leq \frac{\sum_{m=1}^{M} \eta\hat{\tau}p_m^E |\boldsymbol{f}_m^H \boldsymbol{h}_k^d + \boldsymbol{f}_m^H \boldsymbol{V}_k \Theta^E|^2}{1-\hat{\tau}},$$
$$\forall k \in \mathcal{K}, \tag{11a}$$
$$\xi_k \geq 0, \quad \forall k \in \mathcal{K}. \tag{11b}$$

It is readily seen that the energy harvested by the wireless devices may increase after solving Problem $\mathcal{P}2$-2$'$, which implies that the channel gain of the reflection link is enhanced. Then, a reduced power of energy signals can be guaranteed, when we turn back to solve Problem $\mathcal{P}2$-1. As such, a faster convergence can be obtained. However, at a glance of Problem $\mathcal{P}2$-2$'$, Constraint (11a) is still non-convex regarding Θ^E. To tackle this issue, we manipulate the optimization problem in light of [33] as follows. Firstly, we transform Problem $\mathcal{P}2$-2$'$ to its equivalent problem below, by introducing a set of auxiliary variables $\boldsymbol{y}^E$, $\boldsymbol{a}^E$ and $\boldsymbol{b}^E$

$\mathcal{P}2$-2$'$E1 :

$$\max_{\Theta^E, \{\xi_k\}, \boldsymbol{y}^E, \boldsymbol{a}^E, \boldsymbol{b}^E} \sum_{k=1}^{K} \xi_k$$
$$\text{s.t.} \quad (6c), (11b),$$

$$\xi_k + \kappa f_k^2 + \sum_{m=1}^{M} \alpha_{k,m}(p_{k,m}^I + p_c)$$
$$\leq \frac{\sum_{m=1}^{M} \eta\hat{\tau}p_m^E y_{k,m}^E}{1-\hat{\tau}}, \quad \forall k \in \mathcal{K}, \tag{12a}$$
$$a_{k,m}^E = \Re\{\boldsymbol{f}_m^H \boldsymbol{h}_k^d + \boldsymbol{f}_m^H \boldsymbol{V}_k \Theta^E\},$$
$$k \in \mathcal{K}, \ m \in \mathcal{M}, \tag{12b}$$
$$b_{k,m}^E = \Im\{\boldsymbol{f}_m^H \boldsymbol{h}_k^d + \boldsymbol{f}_m^H \boldsymbol{V}_k \Theta^E\},$$
$$k \in \mathcal{K}, \ m \in \mathcal{M}, \tag{12c}$$
$$y_{k,m}^E \leq (a_{k,m}^E)^2 + (b_{k,m}^E)^2,$$
$$k \in \mathcal{K}, \ m \in \mathcal{M}, \tag{12d}$$

where $\Re\{\bullet\}$ and $\Im\{\bullet\}$ represent the real and imaginary part of $\bullet$, respectively. Following this, the successive convex approximation (SCA) method [49] is applied for tackling the non-convex constraint (12d). Specifically, the approximation function is constructed as follows. The right hand side of (12d) is lower-bounded by its first-order approximation at $(\tilde{a}_{k,m}^E, \tilde{b}_{k,m}^E)$, i.e. $(a_{k,m}^E)^2 + (b_{k,m}^E)^2 \geq \tilde{a}_{k,m}^E(2a_{k,m}^E - \tilde{a}_{k,m}^E) + \tilde{b}_{k,m}^E(2b_{k,m}^E - \tilde{b}_{k,m}^E)$, where the equality holds only when we have $\tilde{a}_{k,m}^E = a_{k,m}^E$ and $\tilde{b}_{k,m}^E = b_{k,m}^E$. Now we consider the following optimization problem

$\mathcal{P}2$-2$'$E2 :

$$\max_{\Theta^E, \{\xi_k\}, \boldsymbol{y}^E, \boldsymbol{a}^E, \boldsymbol{b}^E} \sum_{k=1}^{K} \xi_k$$
$$\text{s.t.} \quad (6c), (11b), (12a), (12b), (12c),$$

Algorithm 1 SCA Approach to Design Θ^E, Given the Settings of the Time Allocation, the Computing Phase and the Power Allocation at the WET Phase

Input: $t_{max}, \epsilon, K, M, N, T, \eta, c_k, \kappa, f_{max}, p_c, \Gamma, L_k, \{\boldsymbol{h}_k^d\}$, $\{\boldsymbol{V}_k\}, \hat{\tau}, \boldsymbol{P}^E, \boldsymbol{f}, \{\boldsymbol{\alpha}_k\}, \{\boldsymbol{p}_k^I\}, \Theta^I$ and $\tilde{\Theta}^E$
Output: Θ^E
  1. Initialization
  Initialize $t_1 = 0$; $\epsilon_1 = 1$; $\xi_k = 0, \forall k \in \mathcal{K}$
  2. SCA approach to design Θ^E
  while $t_1 < t_{\max}$ && $\epsilon_1 > \epsilon$ **do**
    • Set $\tilde{a}_{k,m}^E = \Re\{\boldsymbol{f}_m^H \boldsymbol{h}_k^d + \boldsymbol{f}_m^H \boldsymbol{V}_k \tilde{\Theta}^E\}$ and $\tilde{b}_{k,m}^E = \Im\{\boldsymbol{f}_m^H \boldsymbol{h}_k^d + \boldsymbol{f}_m^H \boldsymbol{V}_k \tilde{\Theta}^E\}, \forall k \in \mathcal{K}, \forall m \in \mathcal{M}$
    • Obtain Θ^E and $\{\xi_k\}$ by solving Problem $\mathcal{P}2$-2$'$E2 using CVX
    • Set $\epsilon_1 = \frac{|\text{obj}(\Theta^E) - \text{obj}(\tilde{\Theta}^E)|}{|\text{obj}(\Theta^E)|}$, $\tilde{\Theta}^E \leftarrow \Theta^E$, $t_1 \leftarrow t_1 + 1$
  end while
  3. Output optimal Θ^{E*}
  $\Theta^{E*} \leftarrow \tilde{\Theta}^E$

Algorithm 2 Alternating Optimization of $\boldsymbol{p}^E$ and Θ^E, Given the Settings of the Time Allocation and the Computing Phase

Input: $t_{max}, \epsilon, K, M, N, T, \eta, c_k, \kappa, f_{max}, p_c, \Gamma, L_k, \{\boldsymbol{h}_k^d\}$, $\{\boldsymbol{V}_k\}, \hat{\tau}, \boldsymbol{f}, \{\boldsymbol{\alpha}_k\}, \{\boldsymbol{p}_k^I\}, \Theta^I$ and $\tilde{\Theta}^E$
Output: $\boldsymbol{P}^E$ and Θ^E
  1. Initialization
  • Initialize $t_2 = 0$; $\epsilon_2 = 1$; $\Theta^{E(0)} = \tilde{\Theta}^E$
  • Given $\Theta^{E(0)}$, find $\boldsymbol{P}^{E(0)}$ by solving Problem $\mathcal{P}2$-1 via CVX
  2. Alternating optimization of $\boldsymbol{P}^E$ and Θ^E
  while $t_2 < t_{\max}$ && $\epsilon_2 > \epsilon$ **do**
    • Given $\boldsymbol{P}^{E(t_2)}$ and $\tilde{\Theta}^E = \Theta^{E(t_2)}$, find $\Theta^{E(t_2+1)}$ by solving Problem $\mathcal{P}2$-2$'$E1 using Algorithm 1
    • Given $\Theta^{E(t_2+1)}$, find $\boldsymbol{P}^{E(t_2+1)}$ by solving Problem $\mathcal{P}2$-1 via CVX
    • Set $\epsilon_2 = \frac{|\text{obj}(\boldsymbol{p}^{E(t_2+1)}, \Theta^{E(t_2+1)}) - \text{obj}(\boldsymbol{p}^{E(t_2)}, \Theta^{E(t_2)})|}{|\text{obj}(\boldsymbol{p}^{E(t_2+1)}, \Theta^{E(t_2+1)})|}$,
    $t_2 \leftarrow t_2 + 1$
  end while
  3. Output optimal $\boldsymbol{P}^{E*}$ and Θ^{E*}
  $\Theta^{E*} \leftarrow \Theta^{E(t_2)}$ and $\boldsymbol{P}^{E*} \leftarrow \boldsymbol{P}^{E(t_2)}$

$$y_{k,m}^E = \tilde{a}_{k,m}^E(2a_{k,m}^E - \tilde{a}_{k,m}^E) + \tilde{b}_{k,m}^E(2b_{k,m}^E - \tilde{b}_{k,m}^E), \quad k \in \mathcal{K}, m \in \mathcal{M}. \tag{13a}$$

Both the OF and contraints in Problem $\mathcal{P}2$-2$'$E2 are affine. Hence, Problem $\mathcal{P}2$-2$'$E2 is a convex optimization problem, which can be solved by the implementation of interior-point methods, e.g. CVX [47]. Then, a locally optimal solution of $\mathcal{P}2$-2$'$ can be approached by successively updating $\tilde{a}_{k,m}^E$ and $\tilde{b}_{k,m}^E$ based on the optimal solution of Problem $\mathcal{P}2$-2$'$E2, whose procedure is detailed in Algorithm 1. The computation complexity of the SCA method is analyzed as follows.

Problem $\mathcal{P}2\text{-}2'E2$ involves $2KM$ linear equality constraints (equivalently $4KM$ inequality constraints) of size $2N+1$, K linear inequality constraints of size $M+1$, KM linear inequality constraints of size 3, K linear inequality constraints of size 1, N second-order cone inequality constraints of size 2. Hence, the total complexity of Algorithm 1 is given by $\ln(1/\epsilon)\sqrt{4KM(2N+1)+K(M+1)+3KM+K+2N}$ $(2N+3M+K)\{4KM(2N+1)^3+K(M+1)^3+27KM+K+(2N+3M+K)[4KM(2N+1)^2+K(M+1)^2+9KM+K]+4N+(2N+3M+K)^2\}$ [48], i.e. $\ln(1/\epsilon)\mathcal{O}(K^{1.5}M^{1.5}N^{4.5}+K^{1.5}M^{2.5}N^{3.5}+K^{1.5}M^{2.5}N^{1.5}+K^{2.5}M^{1.5}N^{3.5}+K^{1.5}M^{4.5}+K^{2.5}M^{2.5}N^{2.5}+K^{2.5}M^{3.5}+K^{3.5}M^{1.5}N^{2.5}+K^{3.5}M^{2.5})$. To this end, we summarize the procedure of solving Problem $\mathcal{P}2$ in Algorithm 2.

C. Design of the Computing Phase While Fixing the Time Allocation and WET Settings

In this subsection, we aim for optimizing the design of the computing phase, while fixing the time allocation $\hat{\tau}$ and the WET settings $\boldsymbol{p}^E$ and $\boldsymbol{\Theta}^E$. In this case, we simplify Problem $\mathcal{P}1$ as

$$\mathcal{P}3: \quad \min_{\boldsymbol{f},\{\boldsymbol{\alpha}_k\},\{\boldsymbol{p}_k^I\},\boldsymbol{\Theta}^I} \vartheta \sum_{k=1}^{K}\left[L_k - \frac{(1-\hat{\tau})Tf_k}{c_k}\right]$$

$$\text{s.t. } (6d),(6e),(6f),(6g),(6h),(6i),$$

$$\sum_{m=1}^{M}\alpha_{k,m}B\log_2\left[1+\frac{p_{k,m}|C_{k,m}(\boldsymbol{\Theta}^I)|^2}{\Gamma\sigma^2}\right]$$

$$\geq \frac{L_k - \frac{(1-\hat{\tau})Tf_k}{c_k}}{(1-\hat{\tau})T}, \quad \forall k \in \mathcal{K}. \qquad (14a)$$

Constraint (14a) is not jointly convex regarding $\{\boldsymbol{\alpha}_k\}$, $\{\boldsymbol{p}_k^I\}$ and $\boldsymbol{\Theta}^I$. Hence, it is difficult to find its globally optimal solution. Alternatively, its suboptimal solution is provided by iteratively optimizing the $\boldsymbol{f}$, $\{\boldsymbol{\alpha}_k\}$, $\{\boldsymbol{p}_k^I\}$ and $\boldsymbol{\Theta}^I$, again relying on the AO technique, as follows.

1) Alternating Optimization of the Sub-Band-Device Association and the Power Allocation as Well as the IRS Reflection Coefficient at the Computing Phase: Given a fixed local CPU frequency setting $\boldsymbol{f}$, the OF of Problem $\mathcal{P}3$ becomes deterministic. In other words, the optimization of $\{\boldsymbol{\alpha}_k\}$, $\{\boldsymbol{p}_k^I\}$ and $\boldsymbol{\Theta}^I$ seems not contributing to reducing the OF. However, this is not always true, because if a larger feasible set of $\boldsymbol{f}$ can be obtained by optimizing $\{\boldsymbol{\alpha}_k\}$, $\{\boldsymbol{p}_k^I\}$ and $\boldsymbol{\Theta}^I$, a reduced OF may be achieved when we turn back to optimize $\boldsymbol{f}$. Based on this observation, we formulate the problem below, by introducing a set of auxiliary variables $\{\zeta_k\}$

$$\mathcal{P}3\text{-}1:$$
$$\max_{\{\zeta_k\},\{\boldsymbol{\alpha}_k\},\{\boldsymbol{p}_k^I\},\boldsymbol{\Theta}^I} \sum_{k=1}^{K}\zeta_k$$
$$\text{s.t. } (6e),(6f),(6g),(6h),(14a)$$
$$\zeta_k \geq 0, \quad \forall k \in \mathcal{K}, \qquad (15a)$$
$$(1-\hat{\tau})T\left[\kappa f_k^2 + \sum_{m=1}^{M}\alpha_{k,m}(p_{k,m}^I+p_c)+\zeta_k\right]$$
$$\leq \sum_{m=1}^{M}\eta\hat{\tau}Tp_m^E|C_{k,m}(\boldsymbol{\Theta}^E)|^2, \quad \forall k \in \mathcal{K}. \qquad (15b)$$

As specified in (15a), the auxiliary variables $\{\zeta_k\}$ are non-negative, and thus a non-smaller set of $\boldsymbol{f}$ may be obtained after solving Problem $\mathcal{P}3\text{-}1$. Given that Constraint (14a) is not jointly convex regarding $\{\boldsymbol{p}_k\}$ and $\boldsymbol{\Theta}^I$, we optimize $\{\boldsymbol{\alpha}_k\}$, $\{\boldsymbol{p}_k^I\}$ and $\boldsymbol{\Theta}^I$ in two steps iteratively.

In the first step, we optimize $\{\zeta_k\}$, $\{\boldsymbol{\alpha}_k\}$ and $\{\boldsymbol{p}_k^I\}$, while fixing the IRS reflection coefficient $\boldsymbol{\Theta}^I$. In this case, Problem $\mathcal{P}3\text{-}1$ can be simplified as

$$\mathcal{P}3\text{-}1a: \quad \max_{\{\zeta_k\},\{\boldsymbol{\alpha}_k\},\{\boldsymbol{p}_k^I\}} \sum_{k=1}^{K}\zeta_k$$
$$\text{s.t. } (6e),(6f),(6g),(14a),(15a),(15b). \qquad (16a)$$

Problem $\mathcal{P}3\text{-}1a$ is a combinatorial optimization problem, where the binary constraint (6e) is non-convex. The classic solution typically relies on the convex relaxation method [50], where the binary constraint imposed on $\{\boldsymbol{\alpha}_k\}$ is relaxed into a convex constraint by introducing time-sharing variables. However, the relaxed problem is different from the original problem, which might lead to a specific error. To address this issue, a near-optimal solution based on the Lagrangian duality was proposed in [42], where it is verified that the duality gap vanishes in the system equipped with more than 8 sub-bands [51], [52]. Hence, in this paper, the Lagrangian duality method [53] is invoked for solving Problem $\mathcal{P}3\text{-}1a$. Specifically, denoting the non-negative Lagrange multiplier vectors by $\boldsymbol{\lambda}=[\lambda_1,\lambda_2,\ldots,\lambda_K]^T$ and $\boldsymbol{\mu}=[\mu_1,\mu_2,\ldots,\mu_K]^T$, we formulate the Lagrangian function of Problem $\mathcal{P}3\text{-}1a$ over the domain $\mathcal{D}$ as

$$\mathcal{L}\big(\{\zeta_k\},\{\boldsymbol{p}_k^I\},\boldsymbol{\lambda},\boldsymbol{\mu}\big)$$
$$= \sum_{k=1}^{K}\zeta_k - \sum_{k=1}^{K}\lambda_k\left[\kappa f_k^2 + \sum_{m=1}^{M}(p_{k,m}^I+p_c)+\zeta_k\right.$$
$$\left. - \frac{E_k(\hat{\tau},\boldsymbol{p}^E,\boldsymbol{\Theta}^E)}{(1-\hat{\tau})T}\right]$$
$$+ \sum_{k=1}^{K}\mu_k\left[\sum_{m=1}^{M}B\log_2\left(1+\frac{p_{k,m}^I|C_{k,m}(\boldsymbol{\Theta}^I)|^2}{\Gamma\sigma^2}\right)\right.$$
$$\left. - \frac{L_k - \frac{(1-\hat{\tau})Tf_k}{c_k}}{(1-\hat{\tau})T}\right], \qquad (17)$$

where the domain $\mathcal{D}$ is defined as the set of all non-negative $p_{k,m}^I$ for $\forall k \in \mathcal{K}$ and for $\forall m \in \mathcal{M}$ such that for each m, only a single $p_{k,m}^I$ is positive for $k \in \mathcal{K}$. Then, the Lagrangian dual function of Problem $\mathcal{P}3\text{-}1a$ is given by

$$\mathcal{G}(\boldsymbol{\lambda},\boldsymbol{\mu}) = \max_{\{\zeta_k\},\{\boldsymbol{p}_k^I\}\in\mathcal{D}} \mathcal{L}\big(\{\zeta_k\},\{\boldsymbol{p}_k^I\},\boldsymbol{\lambda},\boldsymbol{\mu}\big). \qquad (18)$$

(18) can be reformulated as

$$\mathcal{G}(\boldsymbol{\lambda},\boldsymbol{\mu})$$
$$= \sum_{m=1}^{M}\hat{\mathcal{G}}_m(\boldsymbol{\lambda},\boldsymbol{\mu}) + \sum_{k=1}^{K}(1-\lambda_k)\zeta_k - \sum_{k=1}^{K}\lambda_k\kappa f_k^2$$
$$+ \sum_{k=1}^{K}\lambda_k\frac{E_k(\hat{\tau},\boldsymbol{p}^E,\boldsymbol{\Theta}^E)}{(1-\hat{\tau})T} - \sum_{k=1}^{K}\frac{\mu_k\left[L_k - \frac{(1-\hat{\tau})Tf_k}{c_k}\right]}{(1-\hat{\tau})T}, \qquad (19)$$

where we have

$$
\hat{\mathcal{G}}_m(\boldsymbol{\lambda}, \boldsymbol{\mu}) \triangleq \max_{\{\boldsymbol{p}_k^I\} \in \mathcal{D}} \left\{ -\sum_{k=1}^K \lambda_k(p_{k,m}^I + p_c) + \sum_{k=1}^K \mu_k B \log_2 \left[1 + \frac{p_{k,m}^I |C_{k,m}(\boldsymbol{\Theta}^I)|^2}{\Gamma \sigma^2} \right] \right\}.
$$
(20)

It is readily seen that (20) is concave regarding $p_{k,m}^I$. Thus, upon letting its first-order derivative regarding $p_{k,m}^I$ be 0, we may give the optimal power of the m-th sub-band when it is allocated to the k-th device as

$$
\hat{p}_{k,m}^I(\lambda_k, \mu_k) = \left[\frac{\mu_k B}{\lambda_k \ln 2} - \frac{\Gamma \sigma^2}{|C_{k,m}(\boldsymbol{\Theta}^I)|^2} \right]^+.
$$
(21)

Then, $\hat{\mathcal{G}}_m(\boldsymbol{\lambda}, \boldsymbol{\mu})$ can be obtained, by searching over all possible assignments of the m-th sub-band for all the K devices, as follows

$$
\hat{\mathcal{G}}_m(\boldsymbol{\lambda}, \boldsymbol{\mu}) = \max_k \left\{ -\lambda_k \left[\hat{p}_{k,m}^I(\lambda_k, \mu_k) + p_c \right] + \mu_k B \log_2 \left[1 + \frac{\hat{p}_{k,m}^I(\lambda_k, \mu_k)|C_{k,m}(\boldsymbol{\Theta}^I)|^2}{\Gamma \sigma^2} \right] \right\},
$$
(22)

and the suitable device is given by $k^* = \arg \hat{\mathcal{G}}_m(\boldsymbol{\lambda}, \boldsymbol{\mu})$. We set $\alpha_{k^*,m} = 1$ and $p_{k^*,m}^I = \hat{p}_{k^*,m}^I$ as well as $\alpha_{k,m} = 0$ and $p_{k,m}^I = 0$ for $\forall k \neq k^*$. We continue by calculating $\{\zeta_k\}$ as follows. At a glance of (21), it is observed that λ_k has to yield $\lambda_k > 0$, $\forall k \in \mathcal{K}$, which implies that Constraint (15b) is strictly binding for the optimal solution of Problem $\mathcal{P}3\text{-}1a$. Therefore, ζ_k can be set as

$$
\zeta_k = \frac{E_k(\hat{\tau}, \boldsymbol{p}^E, \boldsymbol{\Theta}^E)}{(1 - \hat{\tau})T} - \kappa f_k^2 - \sum_{m=1}^M \alpha_{k,m}(p_{k,m}^I + p_c).
$$
(23)

Once all $\hat{\mathcal{G}}_m(\boldsymbol{\lambda}, \boldsymbol{\mu})$ and ζ_k are obtained, $\mathcal{G}(\boldsymbol{\lambda}, \boldsymbol{\mu})$ can be calculated by (19). Bearing in mind that the obtained $\mathcal{G}(\boldsymbol{\lambda}, \boldsymbol{\mu})$ is not guaranteed to be optimal, we have to find a suitable set of $\boldsymbol{\lambda}$ and $\boldsymbol{\mu}$ that minimize $\mathcal{G}(\boldsymbol{\lambda}, \boldsymbol{\mu})$, which can be realized by the ellipsoid method [53]. More explicitly, the Lagrange multipliers are iteratively updated following their sub-gradients towards their optimal settings. The corresponding sub-gradients are given as follows

$$
s_{\lambda_k} = \kappa f_k^2 + \sum_{m=1}^M \alpha_{k,m}(p_{k,m}^I + p_c) - \frac{E_k(\hat{\tau}, \boldsymbol{p}^E, \boldsymbol{\Theta}^E)}{(1 - \hat{\tau})T},
$$
(24)

$$
s_{\mu_k} = \frac{L_k - \frac{(1-\hat{\tau})T f_k}{c_k}}{(1 - \hat{\tau})T} - \sum_{m=1}^M \alpha_{k,m} B \log_2 \left(1 + \frac{p_{k,m}^I |C_{k,m}(\boldsymbol{\Theta}^I)|^2}{\Gamma \sigma^2} \right).
$$
(25)

Upon denoting the iteration index by t, the Lagrange multipliers are updated obeying $\lambda_k(t+1) = [\lambda_k(t) + \delta_\lambda(t)s_{\lambda_k}]^+$ and $\mu_k(t+1) = [\mu_k(t) + \delta_\mu(t)s_{\mu_k}]^+$, where we set $\delta_\lambda(t) = \delta_\lambda(1)/t$ and $\delta_\mu(t) = \delta_\mu(1)/t$ for ensuring the convergence of the OF. In the problem considered, the ellipsoid method

---

Algorithm 3 Design of $\{\boldsymbol{\alpha}_k\}$ and $\{\boldsymbol{p}_k^I\}$, Given the Settings of $\hat{\tau}$, $\boldsymbol{p}^E$, $\boldsymbol{\Theta}^E$, $\boldsymbol{f}$ and $\boldsymbol{\Theta}^I$

Input: t_{max}, ϵ, K, M, N, T, η, c_k, κ, f_{max}, p_c, Γ, L_k, $\{\boldsymbol{h}_k^d\}$, $\{\boldsymbol{V}_k\}$, $\hat{\tau}$, $\boldsymbol{P}^E$, $\boldsymbol{\Theta}^E$, $\boldsymbol{\Theta}^I$, $\boldsymbol{f}$, $\boldsymbol{\Theta}^I$, $\boldsymbol{\lambda}$ and $\boldsymbol{\mu}$
Output: $\{\zeta_k\}$, $\{\boldsymbol{\alpha}_k\}$, $\{\boldsymbol{p}_k^I\}$
  1. Initialization
  Initialize $t_3 = 0$; $\epsilon_3 = 1$; Calculate $\mathcal{L}^{(0)}$ using (17)
  2. Optimization of $\{\zeta_k\}$, $\{\boldsymbol{\alpha}_k\}$ and $\{\boldsymbol{p}_k^I\}$
  while $t_3 < t_{\max}$ && $\epsilon_3 > \epsilon$ **do**
    for $m = 1 : M$ **do**
      • Calculate $\hat{p}_{k,m}^I$ using (21) for each $\forall k \in \mathcal{K}$
      • Obtain the optimal device $k^* = \arg \hat{\mathcal{G}}_m(\boldsymbol{\lambda}, \boldsymbol{\mu})$ in (22)
      • Set $\alpha_{k^*,m} = 1$ and $p_{k^*,m}^I = \hat{p}_{k^*,m}^I$ as well as $\alpha_{k,m} = 0$ and $p_{k,m}^I = 0$ for $\forall k \neq k^*$
    end for
    • Calculate ζ_k using (23)
    • Calculate $\mathcal{L}^{(t_3+1)}$ using (17)
    • Update $\boldsymbol{\lambda}$ and $\boldsymbol{\mu}$ using the ellipsoid method
    • Set $\epsilon_3 = \frac{\left| \mathcal{L}^{(t_3+1)} - \mathcal{L}^{(t_3)} \right|}{\left| \mathcal{L}^{(t_3+1)} \right|}$, $t_3 \leftarrow t_3 + 1$
  end while
  3. Output optimal $\{\zeta_k\}^*$, $\{\boldsymbol{\alpha}_k\}^*$ and $\{\boldsymbol{p}_k^I\}^*$
  $\{\zeta_k\}^* = \{\zeta_k\}$, $\{\boldsymbol{\alpha}_k\}^* = \{\boldsymbol{\alpha}_k\}$, $\{\boldsymbol{p}_k^I\}^* = \{\boldsymbol{p}_k^I\}$

---

converges in $\mathcal{O}(K^2)$ iterations [42], [53]. Within each iteration, the computational complexity is of $\mathcal{O}(KM)$. Hence, the total computational complexity is given by $\mathcal{O}(MK^3)$. The procedure of this Lagrangian duality method is summarized in Algorithm 3.

In the second step, we optimize the IRS reflection coefficient $\boldsymbol{\Theta}^I$, while fixing the settings of the resource allocation at the computing phase $\{\boldsymbol{\alpha}_k\}$ and $\{\boldsymbol{p}^I\}$. In this case, Problem $\mathcal{P}3\text{-}1$ becomes a feasibility-check problem below

$$
\mathcal{P}3\text{-}1b : \text{Find } \boldsymbol{\Theta}^I
$$
$$
\text{s.t. } (6h), (14a).
$$

The problem can be solved using the approach devised in Section III-B.2, detailed as follows. By introducing a set of auxiliary variables $\{\chi_k\}$, we transform $\mathcal{P}3\text{-}1b$ to the problem below

$$
\mathcal{P}3\text{-}1b' : \max_{\boldsymbol{\Theta}^I, \{\chi_k\}} \sum_{k=1}^K \chi_k
$$
$$
\text{s.t. } (6h),
$$
$$
\chi_k \geq 0, \quad \forall k \in \mathcal{K},
$$
(27a)
$$
\sum_{m=1}^m \alpha_{k,m} B \log_2 \left[1 + \frac{p_{k,m}|C_{k,m}(\boldsymbol{\Theta}^I)|^2}{\Gamma \sigma^2} \right]
$$
$$
\geq \frac{L_k - \frac{(1-\hat{\tau})T f_k}{c_k}}{(1 - \hat{\tau})T} + \chi_k, \quad \forall k \in \mathcal{K}.
$$
(27b)

Constraint (27b) is non-convex regarding $\boldsymbol{\Theta}^I$. To address this issue, firstly we transform Problem $\mathcal{P}3\text{-}1b'$ to its equivalent

form, by introducing a set of auxiliary variables $\boldsymbol{y}^I$, $\boldsymbol{a}^I$ and $\boldsymbol{b}^I$

$\mathcal{P}$3-1$b'E$1 :

$$\max_{\boldsymbol{\Theta}^I, \{\chi_k\}, \boldsymbol{y}^I, \boldsymbol{a}^I, \boldsymbol{b}^I} \sum_{k=1}^{K} \chi_k$$

$$\text{s.t.} \quad \text{(6h), (27a),}$$

$$\sum_{m=1}^{m} \alpha_{k,m} B \log_2 \left(1 + \frac{p_{k,m} y_{k,m}^I}{\Gamma \sigma^2} \right)$$

$$\geq \frac{L_k - \frac{(1-\hat{\tau}) T f_k}{c_k}}{(1-\hat{\tau}) T} + \chi_k, \quad \forall k \in \mathcal{K},$$

$$\tag{28a}$$

$$a_{k,m}^I = \Re\{\boldsymbol{f}_m^H \boldsymbol{h}_k^d + \boldsymbol{f}_m^H \boldsymbol{V}_k \boldsymbol{\Theta}^I\},$$
$$k \in \mathcal{K}, \ m \in \mathcal{M}, \tag{28b}$$

$$b_{k,m}^I = \Im\{\boldsymbol{f}_m^H \boldsymbol{h}_k^d + \boldsymbol{f}_m^H \boldsymbol{V}_k \boldsymbol{\Theta}^I\},$$
$$k \in \mathcal{K}, \ m \in \mathcal{M}, \tag{28c}$$

$$y_{k,m}^I = (a_{k,m}^I)^2 + (b_{k,m}^I)^2,$$
$$k \in \mathcal{K}, m \in \mathcal{M}. \tag{28d}$$

Then, upon invoking the so-called SCA method as detailed in Section III-B.2, we approach the locally optimal solution by solving the problem below in a successive manner

$\mathcal{P}$3-1$b'E$2 :

$$\max_{\boldsymbol{\Theta}^I, \{\chi_k\}} \sum_{k=1}^{K} \chi_k$$

$$\text{s.t.} \quad \text{(6h), (27a), (28a), (28b), (28c),}$$
$$y_{k,m}^I = \tilde{a}_{k,m}^I (2 a_{k,m}^I - \tilde{a}_{k,m}^I)$$
$$+ \tilde{b}_{k,m}^I (2 b_{k,m}^I - \tilde{b}_{k,m}^I), \quad k \in \mathcal{K}, m \in \mathcal{M}.$$

$$\tag{29a}$$

Problem $\mathcal{P}$3-1$b'E$2 is a convex optimization problem, which can be readily solved with the aid of the software of CVX [47]. The computational complexity is the same as that given in Section III-B.2. Note that the optimization of $\{\boldsymbol{\alpha}_k\}$, $\{\boldsymbol{p}_k^I\}$ and $\boldsymbol{\Theta}^I$ not only contributes to reducing the OF of Problem $\mathcal{P}$2, but also leads to a decreased OF of Problem $\mathcal{P}$1 by slacking its constraint (8a). Hence, we may still reduce the OF of Problem $\mathcal{P}$1 by iteratively optimizing the settings of the WET phase and the computing phase, even if $\boldsymbol{f}$ reaches its maximum value.

2) Design of CPU Frequencies: Given the settings of the sub-band-device association $\{\boldsymbol{\alpha}_k\}$, the power allocation $\{\boldsymbol{p}_k^I\}$ and the IRS reflection coefficient $\boldsymbol{\Theta}^I$, Problem $\mathcal{P}$3 can be simplified as

$$\mathcal{P}\text{3-2}: \ \min_{\boldsymbol{f}} \vartheta \sum_{k=1}^{K} \left[L_k - \frac{(1-\hat{\tau}) T f_k}{c_k} \right]$$

$$\text{s.t.} \quad \text{(6d), (15b).} \tag{30a}$$

It can be seen that the OF of Problem $\mathcal{P}$3-2 decreases upon increasing $\boldsymbol{f}$. Hence, upon denoting

$$\hat{f}_k = \sqrt{\frac{\frac{E_k(\hat{\tau}, \boldsymbol{p}^E, \boldsymbol{\Theta}^E)}{(1-\hat{\tau}) T} - \sum_{m=1}^{M} \alpha_{k,m} (p_{k,m}^I + p_c) - \zeta_k}{\kappa}}, \tag{31}$$

the optimal $\boldsymbol{f}$ can be obtained as (32), as shown at the bottom of the next page.

Algorithm 4 Alternating Optimization of $\boldsymbol{f}$, $\{\boldsymbol{\alpha}_k\}$, $\{\boldsymbol{p}_k^I\}$ and $\boldsymbol{\Theta}^I$, Given the Settings of $\hat{\tau}$, $\boldsymbol{p}^E$ and $\boldsymbol{\Theta}^E$

Input: t_{max}, ϵ, K, M, N, T, η, c_k, κ, f_{max}, p_c, Γ, L_k, $\{\boldsymbol{h}_k^d\}$, $\{\boldsymbol{V}_k\}$, $\hat{\tau}$, $\boldsymbol{P}^E$, $\boldsymbol{\Theta}^E$, $\boldsymbol{f}$, and $\tilde{\boldsymbol{\Theta}}^I$

Output: $\{\boldsymbol{\alpha}_k\}$ $\{\boldsymbol{p}_k^I\}$ and $\boldsymbol{\Theta}^I$
  1. Initialization
  - Initialize $t_4 = 0$; $\epsilon_4 = 1$; $\boldsymbol{\Theta}^{I(0)} = \tilde{\boldsymbol{\Theta}}^I$
  - Given $\boldsymbol{\Theta}^{I(0)}$, find $\{\boldsymbol{\alpha}_k\}^{(0)}$ and $\{\boldsymbol{p}_k^I\}^{(0)}$ by solving Problem $\mathcal{P}$3-1a via Algorithm 3
  - Obtain $\boldsymbol{f}^{(0)}$ via (32) and calculate $\text{obj}(\boldsymbol{f}^{(0)})$
  2. Alternating optimization of $\boldsymbol{f}$, $\{\boldsymbol{\alpha}_k\}$, $\{\boldsymbol{p}_k^I\}$ and $\boldsymbol{\Theta}^I$
  while $t_4 < t_{max}$ && $\epsilon_4 > \epsilon$ **do**
  - Given $\{\boldsymbol{\alpha}_k\}^{(t_4)}$, $\{\boldsymbol{p}_k^I\}^{(t_4)}$ and $\tilde{\boldsymbol{\Theta}}^I = \boldsymbol{\Theta}^{I(t_4)}$, find $\boldsymbol{\Theta}^{I(t_4+1)}$ by solving Problem $\mathcal{P}$3-1bE1 via Algorithm 1
  - Given $\boldsymbol{\Theta}^{I(t_4+1)}$, find $\{\boldsymbol{\alpha}_k\}^{(t_4+1)}$ and $\{\boldsymbol{p}_k^I\}^{(t_4+1)}$ by solving Problem $\mathcal{P}$3-1a via Algorithm 3
  - Obtain $\boldsymbol{f}^{(t_4+1)}$ via (32) and calculate $\text{obj}(\boldsymbol{f}^{(t_4+1)})$
  - Set $\epsilon_4 = \frac{|\text{obj}(\boldsymbol{f}^{(t_4+1)}) - \text{obj}(\boldsymbol{f}^{(t_4)})|}{|\text{obj}(\boldsymbol{f}^{(t_4+1)})|}$, $t_4 \leftarrow t_4 + 1$
  end while
  3. Output optimal $\{\boldsymbol{\alpha}_k\}^*$ $\{\boldsymbol{p}_k^I\}^*$ and $\boldsymbol{\Theta}^{I*}$
  $\{\boldsymbol{\alpha}_k\}^* \leftarrow \{\boldsymbol{\alpha}_k\}^{(t_4)}$, $\{\boldsymbol{p}_k^I\}^* \leftarrow \{\boldsymbol{p}_k^I\}^{(t_4)}$ and $\boldsymbol{\Theta}^{I*} \leftarrow \boldsymbol{\Theta}^{I(t_4)}$

The procedure of optimizing $\{\boldsymbol{\alpha}_k\}$, $\{\boldsymbol{p}_k^I\}$, $\boldsymbol{\Theta}^I$ and $\boldsymbol{f}$ is summarized in Algorithm 4. To this end, it is readily to summarize the algorithm solving Problem $\mathcal{P}$1 under a given $\hat{\tau}$ in Algorithm 5, and an appropriate τ is found with the aid of numerical results, as detailed in Section IV-B.

Since the variables are grouped into two sub-blocks, the optimization in Algorithm 5 is decomposed into two layers, which incurs high complexity. In order to resolve this issue, a one-layer optimization scheme is also conceived, where the variables $\boldsymbol{P}^E$, $\boldsymbol{\Theta}^E$, $\boldsymbol{f}$, $\{\boldsymbol{\alpha}_k\}$ $\{\boldsymbol{p}_k^I\}$ and $\boldsymbol{\Theta}^I$ are alternatively optimized in a single loop. Its pseudocode is detailed in Algorithm 6.

Remark 1: The feasibility check problems $\mathcal{P}$2-2, $\mathcal{P}$3 and $\mathcal{P}$3-1b may not explicitly contribute to the convergence of the outer loop. By transforming them to $\mathcal{P}$2-2', to $\mathcal{P}$3-1 and to $\mathcal{P}$3-1b', respectively, we are able to enlarge the feasible space of the optimization problem being iterated. As a benefit, the objective function of the outer loop is monotonic and the convergence of the outer loop is guaranteed.

Remark 2: Given that the SCA technique is invoked in solving $\mathcal{P}$2-2' and $\mathcal{P}$3-1b', their objective functions are not guaranteed to be maximized. As such, the solution obtained by Algorithm 5 does not correspond to a locally optimal solution but can only associate with a saddle point [54, Ch. 2].

IV. NUMERICAL RESULTS

In this section, we present the pertinent numerical results, for evaluating the performance of our proposed IRS-aided WP-MEC design. A top view of the HAP, of the wireless devices and of the IRS are shown in Fig. 3, where the HAP's coverage radius is R and the IRS is deployed at the cell edge. The locations of wireless devices are assumed to

---

Algorithm 5 Two-Layer Optimization of the WET and Computing Phases, Given the Time Allocation

Input: t_{max}, ϵ, K, M, N, T, η, c_k, κ, f_{max}, p_c, Γ, L_k, $\{\boldsymbol{h}_k^d\}$, $\{\boldsymbol{V}_k\}$ and $\hat{\tau}$

Output: $\boldsymbol{P}^E$, $\boldsymbol{\Theta}^E$, $\boldsymbol{f}$, $\{\boldsymbol{\alpha}_k\}$ $\{\boldsymbol{p}_k^I\}$ and $\boldsymbol{\Theta}^I$

  1. Initialization
  - Initialize $t_6 = 0$; $\epsilon_6 = 1$; $\tilde{\boldsymbol{\Theta}}^E$
  - Initialize $\boldsymbol{f}^{(0)}$, $\{\boldsymbol{\alpha}_k\}^{(0)}$, $\{\boldsymbol{p}_k^I\}^{(0)}$ and $\boldsymbol{\Theta}^{I(0)}$ following Section III-A
  - Given $\boldsymbol{f}^{(0)}$, $\{\boldsymbol{\alpha}_k\}^{(0)}$, $\{\boldsymbol{p}_k^I\}^{(0)}$ and $\boldsymbol{\Theta}^{I(0)}$, find $\boldsymbol{P}^{E(0)}$ and $\boldsymbol{\Theta}^{E(0)}$ by solving Problem $\mathcal{P}2$ via Algorithm 2

  2. Alternating optimization of $\boldsymbol{P}^E$, $\boldsymbol{\Theta}^E$, $\boldsymbol{f}$, $\{\boldsymbol{\alpha}_k\}$ $\{\boldsymbol{p}_k^I\}$ and $\boldsymbol{\Theta}^I$

  while $t_5 < t_{\max}$ && $\epsilon_5 > \epsilon$ **do**
  - Given $\boldsymbol{P}^{E(t_5)}$, $\boldsymbol{\Theta}^{E(t_5)}$ and $\tilde{\boldsymbol{\Theta}}^I = \boldsymbol{\Theta}^{I(t_5)}$, find $\boldsymbol{f}^{(t_5+1)}$, $\{\boldsymbol{\alpha}_k\}^{(t_5+1)}$, $\{\boldsymbol{p}_k^I\}^{(t_5+1)}$ and $\boldsymbol{\Theta}^{I(t_5+1)}$ by solving Problem $\mathcal{P}3$ using Algorithm 4
  - Given $\boldsymbol{f}^{(t_5+1)}$, $\{\boldsymbol{\alpha}_k\}^{(t_5+1)}$, $\{\boldsymbol{p}_k^I\}^{(t_5+1)}$, $\boldsymbol{\Theta}^{I(t_5+1)}$ and $\tilde{\boldsymbol{\Theta}}^E = \boldsymbol{\Theta}^{E(t_5)}$, find $\boldsymbol{P}^{E(t_5+1)}$ and $\boldsymbol{\Theta}^{E(t_5+1)}$ by solving Problem $\mathcal{P}2$ via Algorithm 2
  - Set $\epsilon_5 = \dfrac{\left|\text{obj}^{(t_5+1)} - \text{obj}^{(t_5)}\right|}{\left|\text{obj}^{(t_5+1)}\right|}$, $t_5 \leftarrow t_5 + 1$

  end while
  3. Output optimal $\boldsymbol{P}^{E^*}$, $\boldsymbol{\Theta}^{E^*}$, $\boldsymbol{f}^*$, $\{\boldsymbol{\alpha}_k\}^*$ $\{\boldsymbol{p}_k^I\}^*$ and $\boldsymbol{\Theta}^{I^*}$
  $\boldsymbol{P}^{E^*} \leftarrow \boldsymbol{P}^{E(t_5)}$, $\boldsymbol{\Theta}^{E^*} \leftarrow \boldsymbol{\Theta}^{E(t_5)}$, $\boldsymbol{f}^* \leftarrow \boldsymbol{f}^{(t_5)}$, $\{\boldsymbol{\alpha}_k\}^* \leftarrow \{\boldsymbol{\alpha}_k\}^{(t_5)}$, $\{\boldsymbol{p}_k^I\}^* \leftarrow \{\boldsymbol{p}_k^I\}^{(t_5)}$ and $\boldsymbol{\Theta}^{I^*} \leftarrow \boldsymbol{\Theta}^{I(t_5)}$

Algorithm 6 One-Layer Optimization of the WET and Computing Phases, Given the Time Allocation

Input: t_{max}, ϵ, K, M, N, T, η, c_k, κ, f_{max}, p_c, Γ, L_k, $\{\boldsymbol{h}_k^d\}$, $\{\boldsymbol{V}_k\}$, $\hat{\tau}$ and $\tilde{\boldsymbol{\Theta}}^E$

Output: $\boldsymbol{P}^E$, $\boldsymbol{\Theta}^E$, $\boldsymbol{f}$, $\{\boldsymbol{\alpha}_k\}$ $\{\boldsymbol{p}_k^I\}$ and $\boldsymbol{\Theta}^I$

  1. Initialization
  - Initialize $t_6 = 0$; $\epsilon_6 = 1$; $\boldsymbol{\Theta}^{E(0)} = \tilde{\boldsymbol{\Theta}}^E$
  - Initialize $\boldsymbol{f}^{(0)}$, $\{\boldsymbol{\alpha}_k\}^{(0)}$, $\{\boldsymbol{p}_k^I\}^{(0)}$ and $\boldsymbol{\Theta}^{I(0)}$ following Section III-A
  - Given $\boldsymbol{\Theta}^{E(0)}$, find $\boldsymbol{P}^{E(0)}$ by solving Problem $\mathcal{P}2$-1 via CVX and calculate $\text{obj}^{(0)}$

  2. Alternating optimization of $\boldsymbol{P}^E$, $\boldsymbol{\Theta}^E$, $\boldsymbol{f}$, $\{\boldsymbol{\alpha}_k\}$ $\{\boldsymbol{p}_k^I\}$ and $\boldsymbol{\Theta}^I$

  while $t_6 < t_{\max}$ && $\epsilon_6 > \epsilon$ **do**
  - Given $\boldsymbol{P}^{E(t_6)}$, $\boldsymbol{\Theta}^{E(t_6)}$, $\boldsymbol{f}^{(t_6)}$ and $\boldsymbol{\Theta}^{I(t_6)}$, find $\{\boldsymbol{\alpha}_k\}^{(t_6+1)}$ and $\{\boldsymbol{p}_k^I\}^{(t_6+1)}$ by solving Problem $\mathcal{P}3$-$1a$ using Algorithm 3
  - Given $\{\boldsymbol{\alpha}_k\}^{(t_6+1)}$, $\{\boldsymbol{p}_k^I\}^{(t_6+1)}$ and $\boldsymbol{\Theta}^{I(t_6)}$, find $\boldsymbol{\Theta}^{I(t_6+1)}$ by solving Problem $\mathcal{P}3$-$1bE1$ via Algorithm 1
  - Obtain $\boldsymbol{f}^{(t_6+1)}$ via (32) and calculate $\text{obj}^{(t_6+1)}$
  - Set $\epsilon_6 = \dfrac{\left|\text{obj}^{(t_6+1)} - \text{obj}^{(t_6)}\right|}{\left|\text{obj}^{(t_6+1)}\right|}$
  - Given $\boldsymbol{P}^{E(t_6)}$, find $\boldsymbol{\Theta}^{E(t_6+1)}$ by solving Problem $\mathcal{P}2$-$2'E1$ using Algorithm 1
  - Given $\boldsymbol{\Theta}^{E(t_6)}$, find $\boldsymbol{P}^{E(t_6+1)}$ by solving Problem $\mathcal{P}2$-1 via CVX
  - $t_6 \leftarrow t_6 + 1$

  end while
  3. Output optimal $\boldsymbol{P}^{E^*}$, $\boldsymbol{\Theta}^{E^*}$, $\boldsymbol{f}^*$, $\{\boldsymbol{\alpha}_k\}^*$ $\{\boldsymbol{p}_k^I\}^*$ and $\boldsymbol{\Theta}^{I^*}$
  $\boldsymbol{P}^{E^*} \leftarrow \boldsymbol{P}^{E(t_5)}$, $\boldsymbol{\Theta}^{E^*} \leftarrow \boldsymbol{\Theta}^{E(t_5)}$, $\boldsymbol{f}^* \leftarrow \boldsymbol{f}^{(t_5)}$, $\{\boldsymbol{\alpha}_k\}^* \leftarrow \{\boldsymbol{\alpha}_k\}^{(t_5)}$, $\{\boldsymbol{p}_k^I\}^* \leftarrow \{\boldsymbol{p}_k^I\}^{(t_5)}$ and $\boldsymbol{\Theta}^{I^*} \leftarrow \boldsymbol{\Theta}^{I(t_5)}$

---

obey the uniform distribution within a circle, whose radius and locations are specified by r as well as d_1 and d_2, respectively. Their default settings are specified in the block of "System model" in Table II. The efficiency of the energy harvesting η is set as 0.5. As for the communications channel, we consider both the small-scale fading and the large-scale path loss. More explicitly, the small-scale fading is assumed to be independent and identically distributed (i.i.d.) and obey the complex Gaussian distribution associated with zero mean and unit variance, while the path loss in dB is given by

$$\text{PL} = \text{PL}_0 - 10\beta \log_{10}\left(\frac{d}{d_0}\right), \tag{33}$$

where PL_0 is the path loss at the reference distance d_0; β and d denote the path loss exponent of and the distance of the communication link, respectively. Here we use β_{ua}, β_{ui} and β_{ia} to represent the path loss exponent of the links between the wireless devices and the HAP, between the wireless devices and the IRS, as well as between the IRS and the HAP,

respectively.[4] Furthermore, the additive while Gaussian noise associated with zero mean and the variable of σ^2 is imposed both on the energy signals and on the offloading signals. The default values of the parameters are set in the block of "Communications model" in Table II. As for the computing model, the variables of L_k and c_k are assumed to obey the uniform distribution. The offloaded tasks are assumed to be computed in parallel by a large number of CPUs at the edge computing node, where the computing capability of each CPU is $f_e = 10^9$ cycle/s. Then, the energy consumption at the edge for processing the offloaded computational tasks can be

---

[4]We assume that the channel of the direct link between the HAP and devices is hostile (due to an obstruction), while this obstruction can be partially avoided by the IRS-reflection link. Hence, we set a higher value for β_{ua}.

$$
f_k = \begin{cases}
0, & \text{if } \dfrac{E_k(\hat{\tau}, \boldsymbol{p}^E, \boldsymbol{\Theta}^E)}{(1-\hat{\tau})T} - \sum_{m=1}^{M} \alpha_{k,m}(p_{k,m}^I + p_c) - \zeta_k < 0, \\[4mm]
\hat{f}_k, & \text{if } 0 \le \dfrac{E_k(\hat{\tau}, \boldsymbol{p}^E, \boldsymbol{\Theta}^E)}{(1-\hat{\tau})T} - \sum_{m=1}^{M} \alpha_{k,m}(p_{k,m}^I + p_c) - \zeta_k < \kappa f_{max}^2, \\[4mm]
f_{max}, & \text{if } \dfrac{E_k(\hat{\tau}, \boldsymbol{p}^E, \boldsymbol{\Theta}^E)}{(1-\hat{\tau})T} - \sum_{m=1}^{M} \alpha_{k,m}(p_{k,m}^I + p_c) - \zeta_k \ge \kappa f_{max}^2.
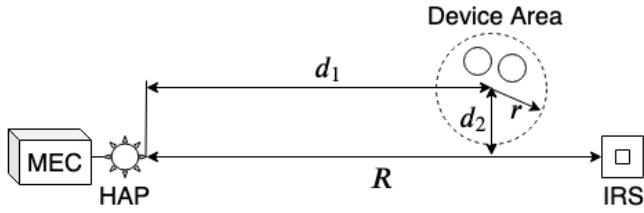\end{cases} \tag{32}
$$

Fig. 3. An illustration of the locations of the HAP, of devices and of the IRS in the IRS-aided WP-MEC system.

TABLE II
DEFAULT SIMULATION PARAMETER SETTING

Description	Parameter and Value
System model [27]	$M = 16$, $N = 30$ $K = 3$, $T = 10$ ms $R = 12$ m, $r = 1$ m $d_1 = 11$ m, $d_2 = 1$ m
Wireless energy transfer model	$\eta = 0.5$
Communication model [33]	$B = 312.5$ KHz $PL_0 = 30$ dB $d_0 = 1$ m $\beta_{ua} = 3.5$ $\beta_{ui} = 2.2$ $\beta_{ia} = 2.2$ $L_k^d = 4$, $L_1 = 2$, $L_{2,k} = 3$ $\sigma^2 = 1.24 \times 10^{-12}$ mW $\Gamma = 2$
Computing model [5]	$L_k = [15, 20]$ Kbit $c_k = [400, 500]$ cycle/bit $f_{max} = 1 \times 10^8$ cycle/s $\kappa = 10^{-28}$ $\vartheta = 5 \times 10^{-8}$ Joule/bit
Convergence criterion	$\epsilon = 0.001$

calculated as $\vartheta = c\kappa f_e^2 = 5 \times 10^{-8}$ Joule/bit. The simulation is operated in a 3.1 GHz processor associated with an 8 GB 2133 MHz memory.

Apart from our algorithms developed in Section III, we also consider two benchmark schemes for comparison. Let us describe these three schemes as follows.

- *With IRS*: In this scheme, we optimize both the power allocation $\boldsymbol{p}^E$ and the IRS reflection coefficients $\boldsymbol{\Theta}^E$ at the WET phase, as well as the local CPU frequency at devices $\boldsymbol{f}$, the sub-band-device association $\{\boldsymbol{\alpha}_k\}$, the power allocation $\{\boldsymbol{p}_k\}$ and the IRS reflection coefficients $\boldsymbol{\Theta}^I$ at the computing phase, relying on Algorithm 5.
- *RandPhase*: The power allocation $\boldsymbol{p}^E$ at the WET phase, as well as the local CPU frequency at devices $\boldsymbol{f}$, the sub-band-device association $\{\boldsymbol{\alpha}_k\}$ and the power allocation $\{\boldsymbol{p}_k\}$ at the computing phase are optimized with the aid of Algorithm 5, while we skip the design of the IRS reflection coefficients $\boldsymbol{\Theta}^E$ and $\boldsymbol{\Theta}^I$, whose amplitude response is set to 1 and phase shifts are randomly set in the range of $[0, 2\pi)$ obeying the uniform distribution.
- *Without IRS*: The composite channel $\boldsymbol{f}_m^H \boldsymbol{V}_k \boldsymbol{\Theta}$ is set to 0 both for the WET and for the computation offloading. The power allocation $\boldsymbol{p}^E$ at the WET phase, as well as the local CPU frequency at devices $\boldsymbol{f}$, the sub-band-device association $\{\boldsymbol{\alpha}_k\}$ and the power allocation $\{\boldsymbol{p}_k\}$

at the computing phase are optimized with the aid of Algorithm 5, while we skip the optimization of the IRS reflection coefficient $\boldsymbol{\Theta}^E$ and $\boldsymbol{\Theta}^I$.

Let us continue by presenting the selection of the time allocation, sub-band allocation in the WET and the computing phases, as well as the impact of diverse environment settings, as follows.

A. Properties of the Proposed Algorithm

1) Convergence Behavior: Fig. 4 presents the convergence behavior of Algorithm 5. It can be seen that the performance of the SCA-aided algorithm proposed for the IRS design converges within 35 iterations, while the outer loops, including the algorithms proposed for solving $\mathcal{P}2$, $\mathcal{P}3$-1 and $\mathcal{P}1$, are capable of achieving a convergence within 5 iterations. Furthermore, as analyzed in Section III, their computational complexity is in a polynomial form. Hence, the proposed algorithm can be practically implemented.

2) Comparison Between Algorithm 5 and Algorithm 6: Fig. 5 depicts the energy consumption performance of Algorithm 5 and of Algorithm 6 in 10 same random channel realizations. It can be seen that Algorithm 5 slightly outperforms Algorithm 6 in most cases. The performance advantage of Algorithm 5 is mainly due to its higher computational complexity. Specifically, our simulation shows that over 100 random channel realizations, the average computation time of Algorithm 5 and of Algorithm 6 spent on each realization are 8.60 s and 41.33 s, respectively, which were run in a 3.1 GHz Intel Core i5 processor. As such, Algorithm 6 is suggested for the practical implementation, because Algorithm 6 has a light performance loss but processes much lower computation complexity.

3) Comparison With the Optimal Joint Sub-Band and Power Allocation Algorithm: Fig. 6 compares the performance of our proposed algorithm with the joint sub-band and power allocation algorithm where the sub-band allocation is optimized using the exhaustive search method and the power allocation is realized by the optimal water-filling algorithm. No performance difference is observed between the exhaustive search and the proposed algorithm, which verifies the zero duality gap. Note that the exhaustive search method requires K^M comparison for the sub-band scheduling, while our proposed algorithm only compares KN candidates. It is demonstrated that our proposed algorithm is capable of achieving a near-optimal performance with dramatically reduced complexity.

4) Impact of the Phase Quantization: Due to the associated hardware limitation, only a limited number of discrete IRS phase shifts can be provided in practice [29], which prohibits the direct implementation of our proposed algorithms. An intuitive practical solution to this issue is to round the continuous phase shift obtained to its nearest discrete phase shift. Naturally, a performance loss is imposed, owing to the associated quantization effect. Fig. 7 evaluates the impact of phase quantization on the total energy consumption, where three assumptions are considered. Specifically, under the assumption of continuous phase shifts, the phase shift of each IRS element
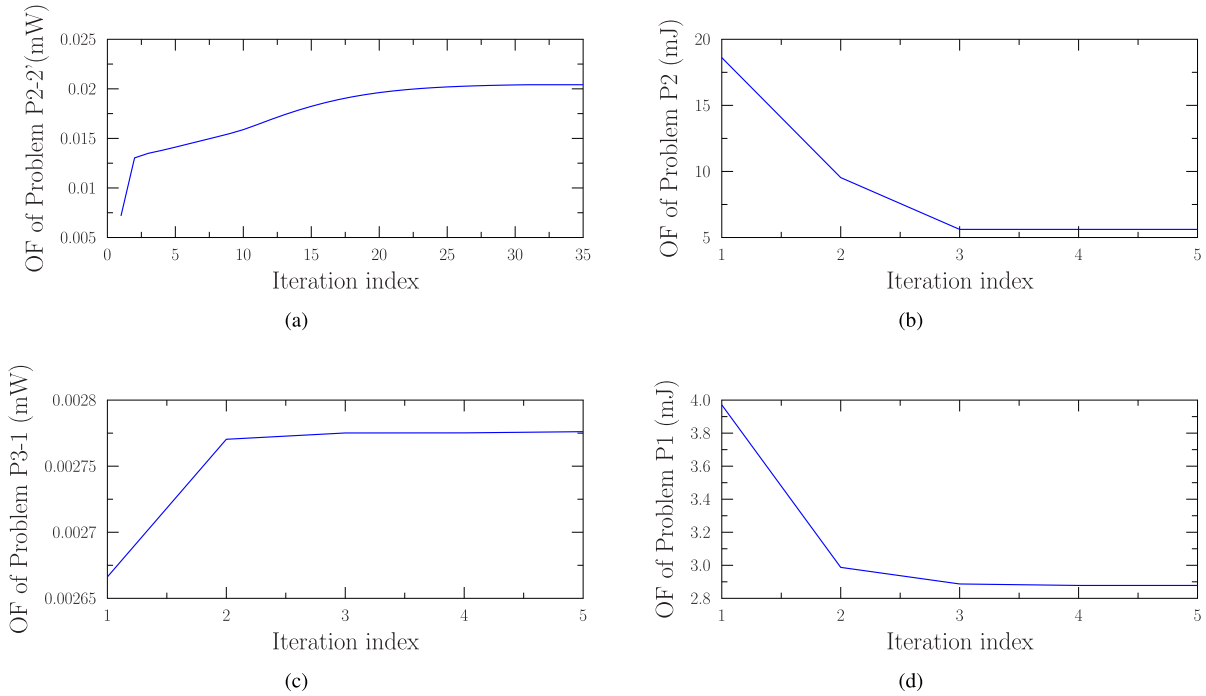
Fig. 4. Convergence behavior of the proposed algorithms. (a) Algorithm 1 for solving Problem $\mathcal{P}2\text{-}2'$; (b) Algorithm 2 for solving Problem $\mathcal{P}2$; (3) Algorithm for solving Problem $\mathcal{P}3\text{-}1$; (d) Algorithm 5 for solving Problem $\mathcal{P}1$. The parameter settings are specified in Table II.
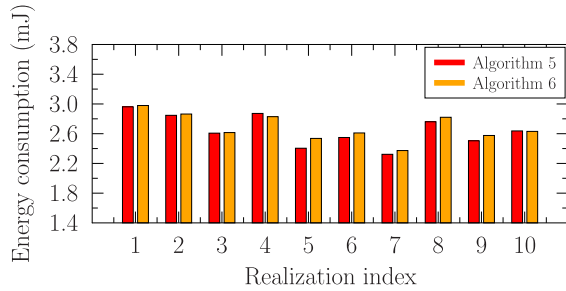

Fig. 5. Simulation results of the total energy consumption versus the realization index by using Algorithm 5 and 6, respectively. The parameter settings are specified in Table II.
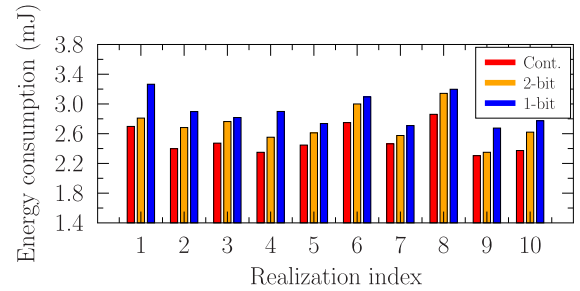
Fig. 7. Simulation results of the total energy consumption versus the realization index under different assumptions of IRS phase shifts. "Cont.", "1-bit" and "2-bit" refer to the assumptions of continuous, 1-bit, and 2-bit phase shifts, respectively. The parameter settings are specified in Table II.
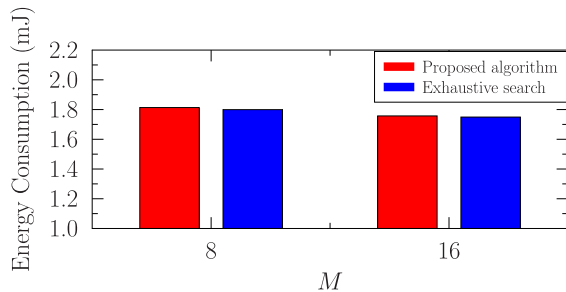
Fig. 6. Simulation results of our proposed algorithm and of the optimal sub-band allocation algorithm. As for the optimal sub-band allocation algorithm, the sub-band allocation makes use of the exhaustive search method and the power allocation is realized by the water-filling algorithm. The number of mobile devices is set as $K = 2$.

can be set as an arbitrary value in the interval of $[0, 2\pi]$; determined by a 1-bit control signal, the phase shift of each IRS element has to be either 0 or π under the assumption of 1-bit phase shift; for a 2-bit control signal, the phase shift of each IRS element has to be one of the values in the set of $\left\{0, \frac{\pi}{2}, \pi, \frac{3\pi}{2}\right\}$. We have the following observations. Firstly, as expected, the total energy consumption decreases upon increasing the number of discrete phase shifts. Secondly, the performance gap between the schemes under the assumptions of continuous phase shifts and 2-bit phase shifts ranges from 1.9% to 10.4%, which implies that the quantization loss is acceptable for 2-bit phase shifts in practice. Therefore, in the following the results obtained under the assumption of the continuous phase are presented for illustrating the best-case performance of the proposed algorithm.

B. Selection of the Time Allocation

In order to find an appropriate time allocation for our WP-MEC system, we depict the total energy consumption (the OF of Problem $\mathcal{P}1$) versus the the time allocation τ
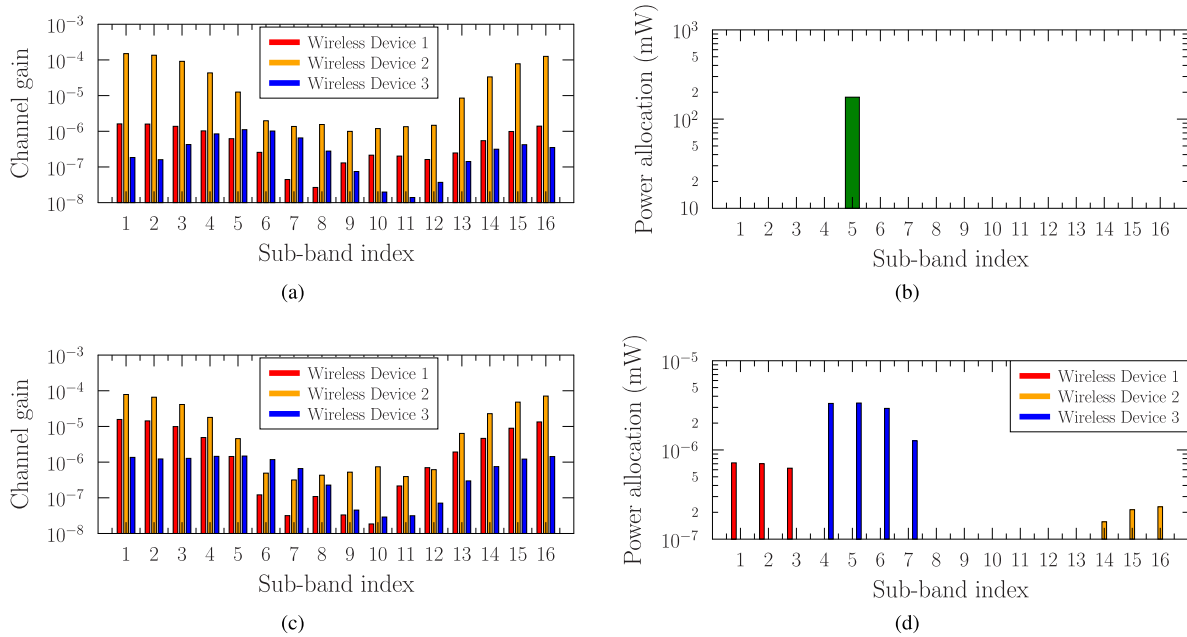
Fig. 8. Joint sub-band and of power allocation for the WET and the computing phases, relying on the Algorithm 5, where the number of bits to be processed is set the same as 20 Kbits for the three wireless devices. (a) The channel gain at the WET phase; (b) The joint sub-band and power allocation at the WET phase; (c) The channel gain at the computing phase; (d) The joint sub-band and power allocation at the computing phase. The parameter settings are specified in Table II.
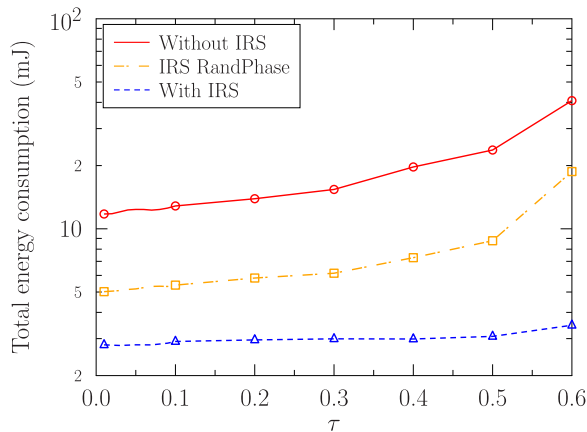

Fig. 9. Simulation results of the total energy consumption versus the time allocation τ relying on the exhaustive search method. The parameter settings are specified in Table II.

in Fig. 9.[5] It can be seen that the total energy consumption becomes higher upon increasing τ for all these three schemes considered. The reason behind it is explained as follows. For a given volume of the computational task to be offloaded within the time duration of T, an increase of τ implies a higher offloading rate required by computation offloading, while at a glance of (5), the computation offloading rate is formulated as a logarithmic function of the offloading power. Hence, we have to largely increase the transmit power of computation offloading for providing the extra offloading rate required by the increase of τ, which results in a higher energy consumption

[5]The exhaustive search for the optimal τ may induce high computational complexity. In practice, τ can be optimized in an offline manner with the aid of simulation results whose parameters are specifically set for the application scenario.

at the wireless devices. Furthermore, since the energy required by WET is determined by the energy consumption at the wireless devices, the total energy consumption becomes higher upon increasing τ. Based on this discussion, it seems that we should select the value of τ as small as possible. However, this may lead to an upsurge of the power consumption for WET, which might exceed the maximum allowable transmit power at the HAP. Therefore, as a compromise, for the environment associated with the default settings we select $\tau = 0.1$, beyond which the total energy consumption becomes increasingly higher along with τ.

C. Joint Sub-Band and Power Allocation in the WET and Computing Phases

Fig. 8 illustrates the channel gain as well as the joint sub-band and power allocation both for the WET and computing phases. Our observations are as follows. Firstly, only a small number of sub-bands are activated for WET. As shown in Fig. 8b, the 5-th sub-band is activated for WET. This allocation is jointly determined by the power consumption of the computing phase and by the channel gain in the WET phase. Specifically, with the reference of Fig. 8d, Device 3 requires the highest power consumption for computation offloading. Given that the overall performance is dominated by the device having the highest energy consumption, we may reduce the energy consumption of WET, by activating the sub-band associated with the highest channel gain of Device 3, which is the 5-th sub-band as shown in Fig. 8a. Secondly, with the reference of Fig. 8c, it can be observed that the power allocation in Fig. 8d obeys the water-filling principle for each device, i.e. allocating a higher power to the sub-band possessing a high channel gain. This corresponds to the power
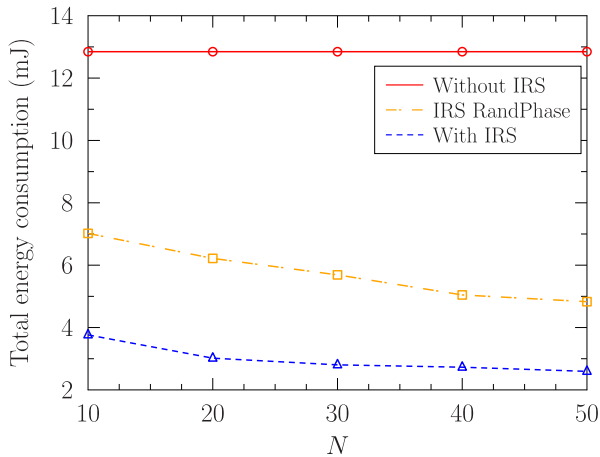
Fig. 10. Simulation results of the total energy consumption versus the number of IRS reflection elements N. The rest of parameters are specified in Table II.

Fig. 11. Simulation results of the total energy consumption versus the distance between the HAP and the wireless device circle d_1. Other parameters are set in Table II.

Fig. 12. Simulation results of the total energy consumption versus the path loss exponent of the IRS reflection link β, where we set $\beta_{ui} = \beta_{ia} = \beta$. Other parameters are set in Table II.

allocation obtained in (21). Thirdly, comparing Fig. 8a and Fig. 8c, we can see that the channel gains in the WET and computing phase are different for each device after we optimize the IRS reflection coefficients, which consolidates our motivation to conceive separate IRS designs for the WET and the computing phases.

D. Performance of the Proposed Solution

In order to evaluate the benefits of employing an IRS in WP-MEC systems, we compare the performance of our proposed algorithms with that of the benchmark schemes, under various settings of the number of IRS reflection elements, of the device location, of the path loss exponent of the IRS-related channel, and of the energy consumption per bit at the edge, as follows.

1) Impact of the Number of IRS Reflection Elements: Fig. 10 shows the simulation results of the total energy consumption versus the number of IRS reflection elements for the three schemes considered. We have the following observations. Firstly, the performance gap between the scheme "Without IRS" and the scheme "IRS RandPhase" increases along with N, which implies that the IRS is capable of assisting the energy consumption reduction in the WP-MEC system, even without carefully designing the IRS reflection coefficients. This is due to the so-called virtual array gain induced by the IRS, as mentioned in Section I. Secondly, the scheme "With IRS" outperforms the scheme "IRS Rand-Phase", which indicates that our sophisticated design of IRS reflection coefficients may provide the so-called passive beam-forming gain for computation offloading. Note that different from the conventional MEC systems [37] where WET is not employed, these two types of gain are exploited twice in WP-MEC systems (during the WET and computing phases, respectively). As such, IRSs are capable of efficiently reducing the energy consumption in WP-MEC systems.

2) Impact of the Distance Between the Device Circle and the IRS: Fig. 11 presents the simulation results of the total energy consumption versus the distance between the HAP and the mobile wireless circles. Our observations are as
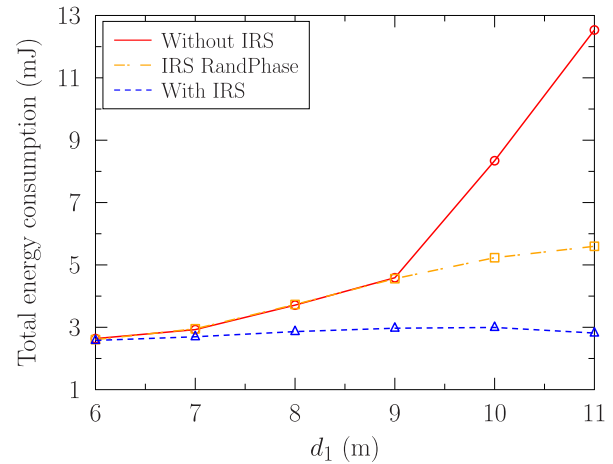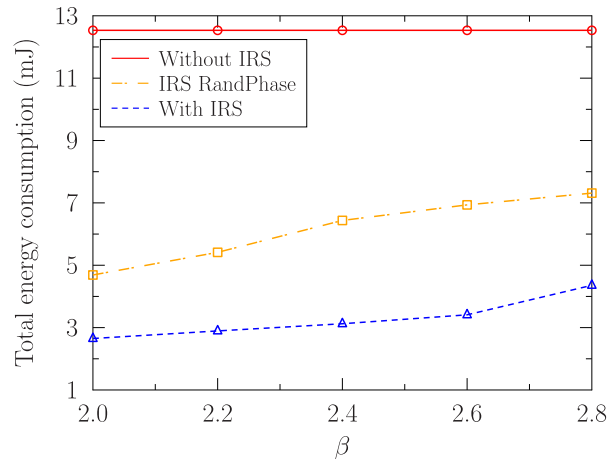
follows. Firstly, the two IRS-aided schemes do not show any visible advantage over the scheme of "Without IRS" when we have $d_1 < 6$ m, which indicates that each IRS has a limited coverage. Secondly, the benefit of deploying the IRS is becomes visible at $d_1 > 9$ m in the scheme of "IRS RandPhase", while the advantage of the "With IRS" scheme is already notable at $d_1 = 7$ m. This observation implies that our sophisticated design of IRS reflection coefficient is capable of extending the coverage of IRS.

3) Impact of Path Loss Exponent: Fig. 12 depicts the simulation results of the total energy consumption versus the path loss exponent of the IRS related links. It can be seen that the total energy consumption decreases if a higher path loss exponent is encountered, which is because a higher β leads to a lower channel gain of the IRS-reflected link. This observation provides an important engineering insight: the locations of IRSs should be carefully selected for avoiding obstacles.

4) Impact of Energy Consumption at the Edge: Fig. 13 shows the simulation results of the total energy consumption versus the energy consumption per bit at the edge node. It can be observed that the advantage of deploying IRS is eminent
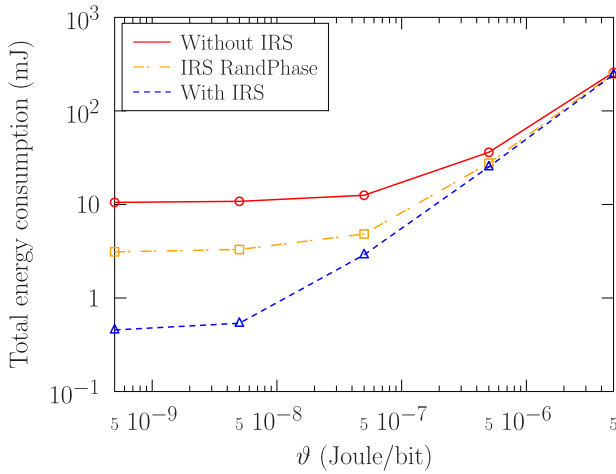
Fig. 13.   Simulation results of the total energy consumption versus the energy consumption per bit at the edge. Other parameters are set in Table II.
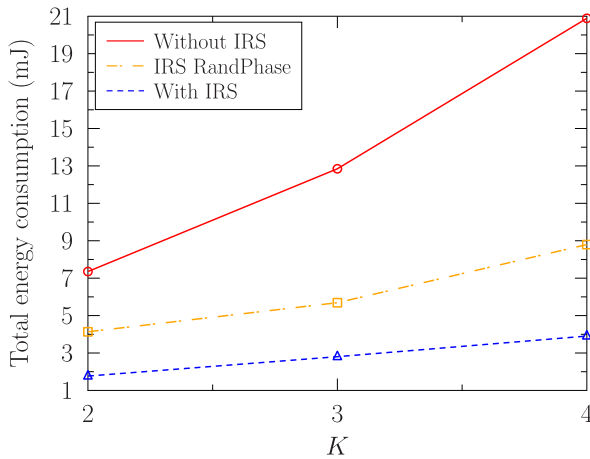

Fig. 14.   Simulation results of the total energy consumption versus the number of mobile devices K. Other parameters are set in Table II.
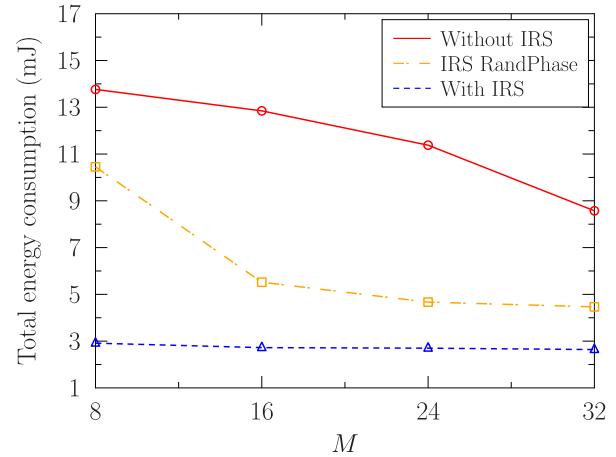

Fig. 15.   Simulation results of the total energy consumption versus the number of sub-bands. Other parameters are set in Table II.

TABLE III
COMPARISON WITH A LOW-COMPLEXITY ALGORITHM. THE DEFAULT
PARAMETERS ARE SET AS SHOWN IN TABLE II

Algorithm	Algorithm 5	The low-complexity algorithm
$N = 20$	$E_{\text{tot}} = 3.02$ mJ	$E_{\text{tot}} = 3.09$ mJ
$N = 30$	$E_{\text{tot}} = 2.80$ mJ	$E_{\text{tot}} = 2.87$ mJ
$N = 40$	$E_{\text{tot}} = 2.73$ mJ	$E_{\text{tot}} = 2.77$ mJ
$K = 2$	$E_{\text{tot}} = 1.77$ mJ	$E_{\text{tot}} = 1.81$ mJ
$K = 3$	$E_{\text{tot}} = 2.80$ mJ	$E_{\text{tot}} = 2.87$ mJ
$K = 4$	$E_{\text{tot}} = 3.91$ mJ	$E_{\text{tot}} = 3.97$ mJ
$M = 8$	$E_{\text{tot}} = 2.91$ mJ	$E_{\text{tot}} = 3.09$ mJ
$M = 16$	$E_{\text{tot}} = 2.80$ mJ	$E_{\text{tot}} = 2.87$ mJ
$M = 32$	$E_{\text{tot}} = 2.64$ mJ	$E_{\text{tot}} = 2.73$ mJ

when we have a small value of ϑ, while the benefit becomes smaller upon increasing the value of ϑ. The reason is explained as follows. The OF of Problem $\mathcal{P}1$ is the combination of the energy consumption of WET and of processing the offloaded computational tasks. If the energy consumption per bit at the edge node is of a small value, the energy consumption of WET plays a dominant role in the total energy consumption. In this case, the benefit of employing IRS is significant. By contrast, if ϑ becomes higher, the total energy consumption is dominated by that at the edge. In this case, although the energy consumption of WET can be degraded by deploying IRSs, this reduction becomes marginal.

5) Impact of the Number of Mobile Devices: Fig. 14 represents the simulation results of the total energy consumption versus the number of mobile devices. It can be observed that although the total energy consumption increases upon increasing the number of mobile devices, the increasing slope of the "With IRS" scheme is the minimum one among those of the three schemes considered. This observation demonstrates the wireless channel can be efficiently reconfigured for achieving a high throughput by carefully designing the IRS reflection

coefficient, even when the average number of sub-bands is limited due to the increase of the mobile devices. This may maintain the total energy consumption as a small value.

6) Impact of the Number of Sub-Bands: Fig. 15 depicts the simulation results of the total energy consumption versus the number of sub-bands. It can be observed that the total energy consumption decreases upon increasing the number of sub-bands. This reason is explained as follows. The increasing number of sub-bands induces at least two benefits. Firstly, the sum of the channel gain may be obtained for each device. Secondly, since the sub-bands are assumed to be independent, the system has a higher possibility to possess a sub-band associated with a large channel gain if M is large. Specific to the "With IRS" scheme, the total energy consumption has a slight decrease when $M = 8$ is changed to $M = 16$, while the reduction of the energy consumption is limited when we have $M > 16$. This is because the energy consumption is dominated by computation offloading when the communications resource is limited, while it is dominated by edge computing when the resource is sufficient.

E. Comparison With a Low-Complexity Algorithm

In order to further reduce the computational complexity of the proposed algorithm, we propose a low-complexity algorithm. Specifically, as seen in Fig. 8, only a single sub-band

is activated for WET. Inspired by this observation, we may firstly calculate the power required by each sub-band when it is activated for WET. Then, the single sub-band associated with the minimum power allocation is selected for WET. The associated complexity is $\mathcal{O}(MK)$, which is much smaller than the complexity of the proposed algorithm. Table III compares the performance of Algorithm 5 and of the low-complexity algorithm. It can be seen that the performance of the proposed low-complexity algorithm is slightly worse than that of Algorithm 5. In practice, this low-complexity algorithm can be invoked.

V. CONCLUSION

To reduce the energy consumption of WP-MEC systems, we have proposed an IRS-aided WP-MEC scheme and formulate an energy minimization problem. A sophisticated algorithm has been developed for optimizing the settings both in the WET and the computing phases. Our numerical results reveal the following insights. Firstly, the employment of IRSs is capable of substantially reducing the energy consumption of the WP-MEC system, especially when the IRS is deployed in vicinity of wireless devices. Secondly, the energy consumption decreases upon increasing the number of IRS reflection elements. Thirdly, the locations of IRSs should be carefully selected for avoiding obstacles. These results inspire us to conceive a low-complexity algorithm for the large-scale IRS-aided WP-MEC system as a future work. Furthermore, as commented in Remark 2, the solution obtained by Algorithm 5 can only associated with a saddle point. In order to further explore the potential of IRS in WP-MEC systems, the optimal design of the IRS phase shift is desired in the future.

REFERENCES

[1] L. Chettri and R. Bera, "A comprehensive survey on Internet of Things (IoT) toward 5G wireless systems," *IEEE Internet Things J.*, vol. 7, no. 1, pp. 16–32, Jan. 2020.

[2] H. Liu, F. Hu, S. Qu, Z. Li, and D. Li, "Multipoint wireless information and power transfer to maximize sum-throughput in WBAN with energy harvesting," *IEEE Internet Things J.*, vol. 6, no. 4, pp. 7069–7078, Aug. 2019.

[3] P. Saffari, A. Basaligheh, V. J. Sieben, and K. Moez, "An RF-powered wireless temperature sensor for harsh environment monitoring with non-intermittent operation," *IEEE Trans. Circuits Syst. I, Reg. Papers*, vol. 65, no. 5, pp. 1529–1542, May 2018.

[4] C. You, K. Huang, and H. Chae, "Energy efficient mobile cloud computing powered by wireless energy transfer," *IEEE J. Sel. Areas Commun.*, vol. 34, no. 5, pp. 1757–1771, May 2016.

[5] F. Wang, J. Xu, X. Wang, and S. Cui, "Joint offloading and computing optimization in wireless powered mobile-edge computing systems," *IEEE Trans. Wireless Commun.*, vol. 17, no. 3, pp. 1784–1797, Mar. 2018.

[6] S. Bi and Y. J. Zhang, "Computation rate maximization for wireless powered mobile-edge computing with binary computation offloading," *IEEE Trans. Wireless Commun.*, vol. 17, no. 6, pp. 4177–4190, Jun. 2018.

[7] J. Feng, Q. Pei, F. R. Yu, X. Chu, and B. Shang, "Computation offloading and resource allocation for wireless powered mobile edge computing with latency constraint," *IEEE Wireless Commun. Lett.*, vol. 8, no. 5, pp. 1320–1323, Oct. 2019.

[8] H. Wu, X. Lyu, and H. Tian, "Online optimization of wireless powered mobile-edge computing for heterogeneous industrial Internet of Things," *IEEE Internet Things J.*, vol. 6, no. 6, pp. 9880–9892, Dec. 2019.

[9] L. Huang, S. Bi, and Y.-J.-A. Zhang, "Deep reinforcement learning for online computation offloading in wireless powered mobile-edge computing networks," *IEEE Trans. Mobile Comput.*, vol. 19, no. 11, pp. 2581–2593, Nov. 2020.

[10] X. Hu, K.-K. Wong, and K. Yang, "Wireless powered cooperation-assisted mobile edge computing," *IEEE Trans. Wireless Commun.*, vol. 17, no. 4, pp. 2375–2388, Apr. 2018.

[11] L. Ji and S. Guo, "Energy-efficient cooperative resource allocation in wireless powered mobile edge computing," *IEEE Internet Things J.*, vol. 6, no. 3, pp. 4744–4754, Jun. 2019.

[12] F. Zhou, Y. Wu, R. Q. Hu, and Y. Qian, "Computation rate maximization in UAV-enabled wireless-powered mobile-edge computing systems," *IEEE J. Sel. Areas Commun.*, vol. 36, no. 9, pp. 1927–1941, Sep. 2018.

[13] Y. Liu, K. Xiong, Q. Ni, P. Fan, and K. B. Letaief, "UAV-assisted wireless powered cooperative mobile edge computing: Joint offloading, CPU control, and trajectory optimization," *IEEE Internet Things J.*, vol. 7, no. 4, pp. 2777–2790, Apr. 2020.

[14] S. Bi, C. K. Ho, and R. Zhang, "Wireless powered communication: Opportunities and challenges," *IEEE Commun. Mag.*, vol. 53, no. 4, pp. 117–125, Apr. 2015.

[15] K. Huang and X. Zhou, "Cutting the last wires for mobile communications by microwave power transfer," *IEEE Commun. Mag.*, vol. 53, no. 6, pp. 86–93, Jun. 2015.

[16] D. Niyato, D. I. Kim, M. Maso, and Z. Han, "Wireless powered communication networks: Research directions and technological approaches," *IEEE Wireless Commun.*, vol. 24, no. 6, pp. 88–97, Dec. 2017.

[17] S. Barbarossa, S. Sardellitti, and P. Di Lorenzo, "Communicating while computing: Distributed mobile cloud computing over 5G heterogeneous networks," *IEEE Signal Process. Mag.*, vol. 31, no. 6, pp. 45–55, Nov. 2014.

[18] W. Shi, J. Cao, Q. Zhang, Y. Li, and L. Xu, "Edge computing: Vision and challenges," *IEEE Internet Things J.*, vol. 3, pp. 637–646, May 2016.

[19] Q. Wu and R. Zhang, "Towards smart and reconfigurable environment: Intelligent reflecting surface aided wireless network," *IEEE Commun. Mag.*, vol. 58, no. 1, pp. 106–112, Jan. 2020.

[20] E. Basar, M. Di Renzo, J. De Rosny, M. Debbah, M. Alouini, and R. Zhang, "Wireless communications through reconfigurable intelligent surfaces," *IEEE Access*, vol. 7, pp. 116753–116773, 2019.

[21] M. Di Renzo *et al.*, "Reconfigurable intelligent surfaces vs. Relaying: Differences, similarities, and performance comparison," 2019, *arXiv:1908.08747*. [Online]. Available: http://arxiv.org/abs/1908.08747

[22] W. Tang *et al.*, "Wireless communications with reconfigurable intelligent surface: Path loss modeling and experimental measurement," 2019, *arXiv:1911.05326*. [Online]. Available: http://arxiv.org/abs/1911.05326

[23] O. Özdogan, E. Björnson, and E. G. Larsson, "Intelligent reflecting surfaces: Physics, propagation, and pathloss modeling," *IEEE Wireless Commun. Lett.*, vol. 9, no. 5, pp. 581–585, May 2020.

[24] Y. Han, W. Tang, S. Jin, C.-K. Wen, and X. Ma, "Large intelligent surface-assisted wireless communication exploiting statistical CSI," *IEEE Trans. Veh. Technol.*, vol. 68, no. 8, pp. 8238–8242, Aug. 2019.

[25] B. Di, H. Zhang, L. Li, L. Song, Y. Li, and Z. Han, "Practical hybrid beamforming with finite-resolution phase shifters for reconfigurable intelligent surface based multi-user communications," *IEEE Trans. Veh. Technol.*, vol. 69, no. 4, pp. 4565–4570, Apr. 2020.

[26] C. Hu and L. Dai, "Two-timescale channel estimation for reconfigurable intelligent surface aided wireless communications," 2019, *arXiv:1912.07990*. [Online]. Available: http://arxiv.org/abs/1912.07990

[27] Y. Yang, B. Zheng, S. Zhang, and R. Zhang, "Intelligent reflecting surface meets OFDM: Protocol design and rate maximization," 2019, *arXiv:1906.09956*. [Online]. Available: http://arxiv.org/abs/1906.09956

[28] Q. Wu and R. Zhang, "Intelligent reflecting surface enhanced wireless network via joint active and passive beamforming," *IEEE Trans. Wireless Commun.*, vol. 18, no. 11, pp. 5394–5409, Nov. 2019.

[29] Q. Wu and R. Zhang, "Beamforming optimization for wireless network aided by intelligent reflecting surface with discrete phase shifts," *IEEE Trans. Commun.*, vol. 68, no. 3, pp. 1838–1851, Mar. 2020.

[30] H. Guo, Y.-C. Liang, J. Chen, and E. G. Larsson, "Weighted sum-rate optimization for intelligent reflecting surface enhanced wireless networks," 2019, *arXiv:1905.07920*. [Online]. Available: http://arxiv.org/abs/1905.07920

[31] G. Zhou, C. Pan, H. Ren, K. Wang, and A. Nallanathan, "A framework of robust transmission design for IRS-aided MISO communications with imperfect cascaded channels," 2020, *arXiv:2001.07054*. [Online]. Available: http://arxiv.org/abs/2001.07054

[32] C. Pan *et al.*, "Multicell MIMO communications relying on intelligent reflecting surface," 2019, *arXiv:1907.10864*. [Online]. Available: http://arxiv.org/abs/1907.10864

[33] Y. Yang, S. Zhang, and R. Zhang, "IRS-enhanced OFDMA: Joint resource allocation and passive beamforming optimization," *IEEE Wireless Commun. Lett.*, vol. 9, no. 6, pp. 760–764, Jun. 2020.

[34] L. Dong and H.-M. Wang, "Secure MIMO transmission via intelligent reflecting surface," *IEEE Wireless Commun. Lett.*, vol. 9, no. 6, pp. 787–790, Jun. 2020.

[35] S. Hong, C. Pan, H. Ren, K. Wang, and A. Nallanathan, "Artificial-Noise-Aided secure MIMO wireless communications via intelligent reflecting surface," 2020, *arXiv:2002.07063*. [Online]. Available: http://arxiv.org/abs/2002.07063

[36] Y. Zheng, S. Bi, Y. J. Zhang, Z. Quan, and H. Wang, "Intelligent reflecting surface enhanced user cooperation in wireless powered communication networks," *IEEE Wireless Commun. Lett.*, vol. 9, no. 6, pp. 901–905, Jun. 2020.

[37] T. Bai, C. Pan, Y. Deng, M. Elkashlan, A. Nallanathan, and L. Hanzo, "Latency minimization for intelligent reflecting surface aided mobile edge computing," 2019, *arXiv:1910.07990*. [Online]. Available: http://arxiv.org/abs/1910.07990

[38] C. Pan *et al.*, "Intelligent reflecting surface aided MIMO broadcasting for simultaneous wireless information and power transfer," 2019, *arXiv:1908.04863*. [Online]. Available: http://arxiv.org/abs/1908.04863

[39] Q. Wu and R. Zhang, "Weighted sum power maximization for intelligent reflecting surface aided SWIPT," *IEEE Wireless Commun. Lett.*, vol. 9, no. 5, pp. 586–590, May 2020.

[40] Y. Tang, G. Ma, H. Xie, J. Xu, and X. Han, "Joint transmit and reflective beamforming design for IRS-assisted multiuser MISO SWIPT systems," 2019, *arXiv:1910.07156*. [Online]. Available: http://arxiv.org/abs/1910.07156

[41] B. Lyu, P. Ramezani, D. T. Hoang, S. Gong, Z. Yang, and A. Jamalipour, "Optimized energy and information relaying in self-sustainable IRS-empowered WPCN," 2020, *arXiv:2004.03108*. [Online]. Available: http://arxiv.org/abs/2004.03108

[42] K. Seong, M. Mohseni, and J. Cioffi, "Optimal resource allocation for OFDMA downlink systems," in *Proc. IEEE Int. Symp. Inf. Theory*, Jul. 2006, pp. 1394–1398.

[43] F. Zhou and R. Q. Hu, "Computation efficiency maximization in wireless-powered mobile edge computing networks," *IEEE Trans. Wireless Commun.*, vol. 19, no. 5, pp. 3170–3184, May 2020.

[44] F. Zhou, Z. Chu, H. Sun, R. Q. Hu, and L. Hanzo, "Artificial noise aided secure cognitive beamforming for cooperative MISO-NOMA using SWIPT," *IEEE J. Sel. Areas Commun.*, vol. 36, no. 4, pp. 918–931, Apr. 2018.

[45] X. Zhang, Y. Wang, F. Zhou, N. Al-Dhahir, and X. Deng, "Robust resource allocation for MISO cognitive radio networks under two practical non-linear energy harvesting models," *IEEE Commun. Lett.*, vol. 22, no. 9, pp. 1874–1877, Sep. 2018.

[46] Y. Wang, M. Sheng, X. Wang, L. Wang, and J. Li, "Mobile-edge computing: Partial computation offloading using dynamic voltage scaling," *IEEE Trans. Commun.*, vol. 64, no. 10, pp. 4268–4282, Oct. 2016.

[47] M. Grant and S. Boyd. (Mar. 2014). *CVX: MATLAB Software for Disciplined Convex Programming, Version 2.1.* [Online]. Available: http://cvxr.com/cvx

[48] K.-Y. Wang, A. M.-C. So, T.-H. Chang, W.-K. Ma, and C.-Y. Chi, "Outage constrained robust transmit optimization for multiuser MISO downlinks: Tractable approximations by conic optimization," *IEEE Trans. Signal Process.*, vol. 62, no. 21, pp. 5690–5705, Nov. 2014.

[49] M. Razaviyayn, "Successive convex approximation: Analysis and applications," Ph.D. dissertation, Dept. Elect. Comput. Eng., Univ. Minnesota, Minneapolis, MN, USA, 2014.

[50] C. Yui Wong, R. S. Cheng, K. B. Lataief, and R. D. Murch, "Multiuser OFDM with adaptive subcarrier, bit, and power allocation," *IEEE J. Sel. Areas Commun.*, vol. 17, no. 10, pp. 1747–1758, Oct. 1999.

[51] W. Yu and R. Lui, "Dual methods for nonconvex spectrum optimization of multicarrier systems," *IEEE Trans. Commun.*, vol. 54, no. 7, pp. 1310–1322, Jul. 2006.

[52] H. Kim, H. Lee, M. Ahn, H.-B. Kong, and I. Lee, "Joint subcarrier and power allocation methods in full duplex wireless powered communication networks for OFDM systems," *IEEE Trans. Wireless Commun.*, vol. 15, no. 7, pp. 4745–4753, Jul. 2016.

[53] S. Boyd and L. Vandenberghe, *Convex Optimization.* Cambridge, U.K.: Cambridge Univ. Press, 2004.

[54] D. P. Bertsekas, "Nonlinear programming," *J. Oper. Res. Soc.*, vol. 48, no. 3, p. 334, 1997.

Tong Bai (Member, IEEE) received the B.Sc. degree in telecommunications from Northwestern Polytechnical University, Xi'an, China, in 2013, and the M.Sc. and Ph.D. degrees in communications and signal processing from the University of Southampton, Southampton, U.K., in 2014 and 2019, respectively. From 2019 to 2020, he was a Post-Doctoral Researcher with the Queen Mary University of London, London, U.K. He is currently an Assistant Professor with Beihang University. His research interests include performance analysis, transceiver design, utility optimization for power-line and wireless communications, and the Internet of Things.

Cunhua Pan (Member, IEEE) received the B.S. and Ph.D. degrees from the School of Information Science and Engineering, Southeast University, Nanjing, China, in 2010 and 2015, respectively.

From 2015 to 2016, he was a Research Associate with the University of Kent, U.K. He held a post-doctoral position with the Queen Mary University of London, U.K., from 2016 and 2019, where he is currently a Lecturer. His research interests include reconfigurable intelligent surfaces (RIS), intelligent reflection surface (IRS), ultra-reliable low latency communication (URLLC), machine learning, UAV, the Internet of Things, and mobile edge computing. He serves as a TPC Member for numerous conferences, such as ICC and GLOBECOM, and the Student Travel Grant Chair for ICC 2019. He is currently an Editor of IEEE WIRELESS COMMUNICATION LETTERS, IEEE COMMUNICATIONS LETTERS and IEEE ACCESS. He also serves as a Leading Guest Editor for the IEEE JOURNAL OF SELECTED TOPICS IN SIGNAL PROCESSING (JSTSP) Special Issue on Advanced Signal Processing for Reconfigurable Intelligent Surface-aided 6G Networks and IEEE ACCESS Special Issue on Reconfigurable Intelligent Surface Aided Communications for 6G and Beyond.

Hong Ren (Member, IEEE) received the B.S. degree in electrical engineering from Southwest Jiaotong University, Chengdu, China, in 2011, and the M.S. and Ph.D. degrees in electrical engineering from Southeast University, Nanjing, China, in 2014 and 2018, respectively. From 2016 to 2018, she was a Visiting Student with the School of Electronics and Computer Science, University of Southampton, U.K. From 2018 to 2020, she was a Post-Doctoral Scholar with the Queen Mary University of London, U.K. She is currently an Associate Professor with Southeast University. Her research interests include communication and signal processing, including green communication systems, cooperative transmission, and cross layer transmission optimization.

Yansha Deng (Member, IEEE) received the Ph.D. degree in electrical engineering from the Queen Mary University of London, U.K., in 2015. From 2015 to 2017, she was a Post-Doctoral Research Fellow with Kings College London, U.K. She is currently a Lecturer (Assistant Professor) with the Department of Engineering, King's College London. Her research interests include molecular communication and machine learning for 5G/B5G wireless networks. She has served as a TPC Member for many IEEE conferences, such as IEEE GLOBECOM and ICC. She was a recipient of the Best Paper Awards from ICC 2016 and Globecom 2017 as the first author. She is currently an Associate Editor of the IEEE TRANSACTIONS ON COMMUNICATIONS and IEEE TRANSACTIONS ON MOLECULAR, BIOLOGICAL AND MULTI-SCALE COMMUNICATIONS, and the Senior Editor of the IEEE COMMUNICATION LETTERS. She also received the Exemplary Reviewers of the IEEE TRANSACTIONS ON COMMUNICATIONS in 2016 and 2017, and IEEE TRANSACTIONS ON WIRELESS COMMUNICATIONS in 2018.

Maged Elkashlan (Member, IEEE) received the Ph.D. degree in electrical engineering from The University of British Columbia, Canada, 2006.

From 2007 to 2011, he was with the Commonwealth Scientific and Industrial Research Organization (CSIRO), Australia. During this time, he held visiting appointments with the University of New South Wales and the University of Technology Sydney. In 2011, he joined the School of Electronic Engineering and Computer Science, Queen Mary University, London, U.K. His research interests include communication theory and statistical signal processing. He received the Best Paper Award from the IEEE International Conference on Communications (ICC) in 2016 and 2014, the International Conference on Communications and Networking in China (CHINACOM) in 2014, and the IEEE Vehicular Technology Conference (VTC-Spring) in 2013. He currently serves as an Editor for IEEE TRANSACTIONS ON WIRELESS COMMUNICATIONS and IEEE TRANSACTIONS ON VEHICULAR TECHNOLOGY.

He received the IEEE Communications Society SPCE Outstanding Service Award 2012 and the IEEE Communications Society RCC Outstanding Service Award 2014. He was a co-recipient of the Best Paper Awards from the IEEE International Conference on Communications 2016 (ICC'2016), the IEEE Global Communications Conference 2017 (GLOBECOM'2017), and the IEEE Vehicular Technology Conference 2018 (VTC'2018). He served as the Chair for the Signal Processing and Communication Electronics Technical Committee of IEEE Communications Society and a Technical Program Chair and a member of Technical Program Committees in numerous IEEE conferences. He serves as an Editor-at-Large for IEEE TRANSACTIONS ON COMMUNICATIONS and a Senior Editor for IEEE WIRELESS COMMUNICATIONS LETTERS. He was an Editor of the IEEE TRANSACTIONS ON WIRELESS COMMUNICATIONS from 2006 to 2011, IEEE TRANSACTIONS ON VEHICULAR TECHNOLOGY from 2006 to 2017, and IEEE SIGNAL PROCESSING LETTERS. He is an IEEE Distinguished Lecturer. He has been selected as a Web of Science Highly Cited Researcher in 2016 and AI 2000 Internet of Things Most Influential Scholar in 2020.

Arumugam Nallanathan (Fellow, IEEE) has been a Professor of Wireless Communications and the Head of the Communication Systems Research (CSR) Group, School of Electronic Engineering and Computer Science, Queen Mary University of London, since September 2017. He was with the Department of Informatics, King's College London, from December 2007 to August 2017, where he was a Professor of Wireless Communications from April 2013 to August 2017 and a Visiting Professor from September 2017. He was an Assistant Professor with the Department of Electrical and Computer Engineering, National University of Singapore, from August 2000 to December 2007. He published nearly 500 technical papers in scientific journals and international conferences. His research interests include artificial intelligence for wireless systems, beyond 5G wireless networks, the Internet of Things (IoT), and molecular communications.